

SUPPORTING INFORMATION

Theoretical and Experimental Characterization of 1,4-N \cdots S σ -hole

Intramolecular Interactions in Bioactive *N*-Acylhydrazone Derivatives

Pedro de Sena Murteira Pinheiro;^{ab} Daniel Alencar Rodrigues;^{ac} Marina Amaral Alves;^{ac} Luzineide Wanderley

Tinoco;^{bd} Glaucio Braga Ferreira;^e Carlos Mauricio Rabello de Sant'Anna;^{af} Carlos Alberto Manssour Fraga^{ab}*

^aLaboratório de Avaliação e Síntese de Substâncias Bioativas (LASSBio), Instituto de Ciências Biomédicas, Universidade Federal do Rio de Janeiro, PO Box 68023, 21941-902, Rio de Janeiro, RJ, Brazil;

^bPrograma de Pós-Graduação em Farmacologia e Química Medicinal, Instituto de Ciências Biomédicas, Universidade Federal do Rio de Janeiro, 21941-902, Rio de Janeiro, RJ, Brazil

^cPrograma de Pós-Graduação em Química, Instituto de Química, Universidade Federal do Rio de Janeiro, 21941-909, Rio de Janeiro, RJ, Brazil;

^dLaboratório de Análise e Desenvolvimento de Inibidores Enzimáticos (LADIE), Instituto de Pesquisa em Produtos Naturais (IPPN), Universidade Federal do Rio de Janeiro, 21941-902, Rio de Janeiro, RJ, Brazil;

^ePrograma de Pós-Graduação em Química, Instituto de Química, Universidade Federal Fluminense, Niterói, Rio de Janeiro, 24020-141, Brazil;

^fDepartamento de Química, Instituto de Ciências Exatas, Universidade Federal Rural do Rio de Janeiro, 23970-000, Seropédica, RJ, Brazil

In this section we describe the theoretical and experimental characterization of the 1,4-N \cdots S σ -hole intramolecular interaction for the compounds 2-(thiophen-2-yl)pyridine (**3**) and **LASSBio-785** (**4**), in comparison with their respective regioisomers at thiophene ring, *i.e.*, 2-(thiophen-3-yl)pyridine (**6**) and **LASSBio-1289** (**5**), which possess similar relationship as for **LASSBio-294** (**1**) and **LASSBio-897** (**2**). In addition, we described the validation process which allowed us to choose the most appropriate method for the theoretical description of the 1,4-N \cdots S σ -hole intramolecular interaction. Beyond that, here we also describe additional data about the 1,4-N \cdots S σ -hole intramolecular interaction characterization of **LASSBio-294** (**1**) in comparison with **LASSBio-897** (**2**).

The description of the results is divided according to the summary below.

1. Validation of the theoretical methodology: (pag 3)

1.1. Computational Details. (pag 3)

1.2. Definition of the basis set for quantum-mechanical calculations. (pag 3)

1.3. Studies of structure-property relationships. (pag 6)

1.4. Evaluation of parameters involved in 1,4-N \cdots S σ -hole intramolecular interactions. (pag 15)

1.5. Influence of adjacent groups in the σ -hole regions. (pag 17)

2. Theoretical and experimental characterization of the 1,4-N \cdots S interaction for the compounds (3**) and (**6**).** (pag 19)

3. Theoretical and experimental characterization of the 1,4-N \cdots S interaction for the compounds **LASSBio-785 (**4**) and **LASSBio-1289** (**5**).** (pag 29)

4. Additional information for the characterization of **LASSBio-294 (**1**) and **LASSBio-897** (**2**).** (pag 38)

5. Spectroscopy acquisition details. (pag 44)

6. Additional theoretical data. (pag 45)

1. Validation of the theoretical methodology.

1.1. Computational Details. At first, we performed a validation process based on **(3)**, since this compound has theoretical^{1,2} and experimental results^{2,3} that helped us in the choice of the most appropriated method to describe the 1,4-N \cdots S σ -hole intramolecular interactions. The validation of the methodology used in the theoretical characterization of molecular modeling studies consisted in four stages: the first stage was the definition of the basis set used for quantum-mechanical calculations. The second one was accomplished through studies of structure-property relationship of the σ -hole regions. The third stage consisted of evaluating specific parameters that may be directly involved in the 1,4-N \cdots S interaction. The fourth stage was carried out through the investigation of the influences of adjacent groups in the size and energy of the σ -hole regions.

1.2. Definition of the basis set for quantum-mechanical calculations. This step was carried out through analysis of the PES scan of **(3)**, considering the dihedral angle N-C-C-S (**Figure S1**) in steps of 30° in the range of 0° to 180°, by 4 levels of theory: semi-empirical (PM6),⁴ two *ab initio*, a Hartree-Fock (HF) type and second order Moller-Plesset (MP2) type, and density functional theory (B3LYP).^{5,6} In the last three methods (HF, MP2 and B3LYP) we used different basis sets, including polarization and diffuse functions (6-31+G(d) / 6-311G(d) / 6-311+G(d,p)). From the lowest energy conformers observed in PES scan analysis equilibrium geometry calculations were performed with no restrictions, maintaining the same method with the same basis set used previously. The resulting geometries were compared to the geometries of the crystallographic structure of **(3)** (CCDC: 1171046)³ in relation to the N \cdots S distance and the N-C-C-S dihedral angle (**Figure S1** and **Tables S1** and **S2**). In the graphs related to PES scan analysis of **(3)**, the 0° dihedral angle refers to the *syn* conformer, where the nitrogen and sulfur atoms are closer to each other, and the 180° dihedral angle is related to the *anti* conformer.

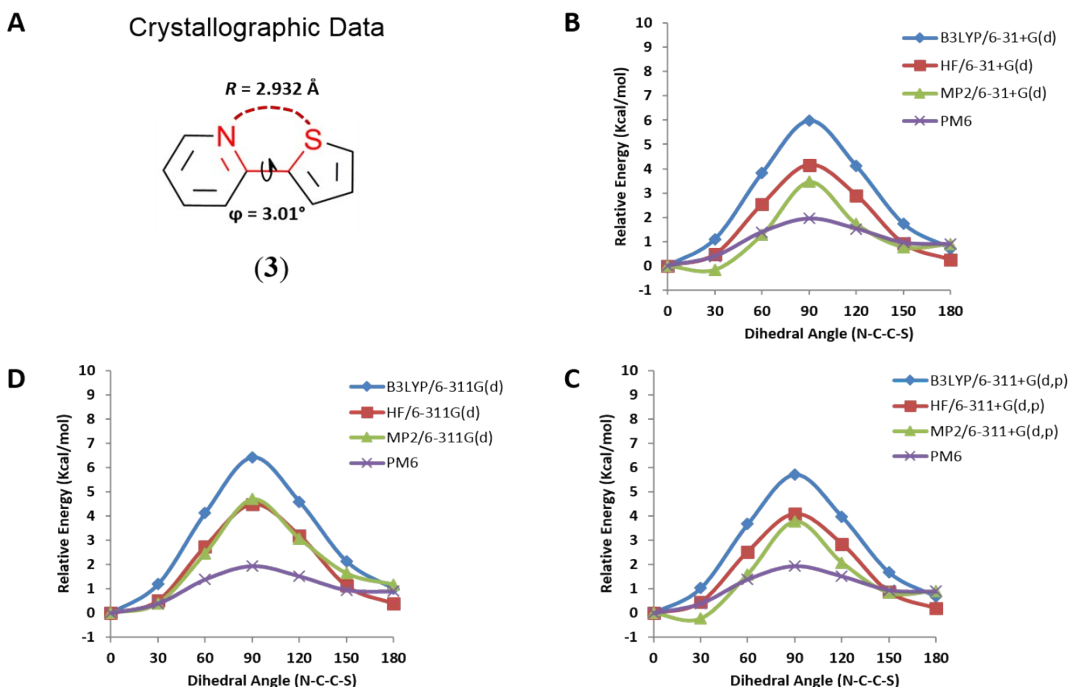


Figure S1. Potential energy surface (PES) scan results of **(3)**. (A) Compound **(3)** chemical structure. The dihedral angle N-C-C-S used in PES analysis is marked in red. Data about crystallographic structure of **(3)** are shown in (N...S Distance and N-C-C-S dihedral angle). CCDC code of **(3)**: 1171046 (Ghosh and Simonsen, 1993). (B) The results of the PES scan analysis for the basis function 6-31+G(d). (C) The results of the PES scan analysis for the basis function 6-311+G(d,p). (D) The results of the PES scan analysis for the basis function 6-311G(d). Legend: blue = B3LYP; green = MP2; red = HF; purple = PM6. All data presented here was obtained through the Spartan'14 software (Wavefunction, Inc.).

When analyzing the graphs shown in **Figure S1**, it is observed that in general, all methods showed a similar behavior, identifying the *syn* conformer as more stable than the *anti* conformer, which is in accordance with the previously published data.^{1,2}

Table S1. *Anti-syn* energy differences evidenced in the PES scan analysis of (**3**). The values are shown in kcal/mol.

Methods	<i>E</i> (<i>Anti-syn</i>) (kcal/mol)			
	Basis set			
	STO-3G	6-31+G(d)	6-311G(d)	6-311+G(d,p)
MP2		0.90	1.17	0.91
HF		0.24	0.39	0.20
B3LYP		0.71	1.00	0.68
PM6	0.89			

However, with the comparative analysis of our own data it can be seen that there are differences depending on the basis set used. It was observed that using the basis set with diffuse functions (6-31+G(d) and 6-311+G(d,p)), the 30° conformer is the most stable one for the MP2 method (the 30° conformer showed a negative relative energy), which was not observed for the 6-311G(d) basis set. In addition, the use of the 6-311G(d) basis set resulted in higher interconversion energy barriers between the *syn* and the *anti* conformers and larger energy difference between these two conformers (*anti-syn*), showing a predicted increased stability for N⋯S interaction when this basis set is used.

Regardless of the method and basis set used, it was observed a decrease in potential energy when the nitrogen and sulfur atoms get closer, which may be an indication that all methods were able to identify the N⋯S interaction. According to our data, in all cases the MP2 was the method that identified the highest stabilities of N⋯S interactions (larger *anti-syn* energy difference). B3LYP was the method that identified the highest interconversion barriers. PM6, despite having identified the smallest barrier, was efficient in identifying the *anti-syn* energy differences, which is interesting since this method has a significantly lower computational cost compared with the *ab initio* and DFT methods, which may be of interest in studies for larger systems.⁴

The data of conformational analysis (**Table S2**) indicated that all methods, regardless the basis set used, produced results close to the geometry observed in the crystals of (**3**). However, using the basis set 6-311G(d) there was a greater resemblance with the experimental data. This fact is more evident when we compare the results of (**3**) for the MP2 method with the three basis sets used. In accordance with the lowest energy conformer detected in the PES scan analysis with each method, the equilibrium geometry calculations with the 6-311G(d) basis set were carried out for the *syn* conformer, whereas for the 6-31+G(d) and 6-311+G(d,p) basis sets, the conformer used for equilibrium geometry calculations was the conformer with the dihedral angle equal to 30°. Then, according to our

data, the 6-311G(d) basis set appeared to be more suitable for carrying out our studies of molecular modeling, and this basis set was chosen to proceed with the theoretical characterization of 1,4-N \cdots S σ -hole intramolecular interactions.

Table S2. Comparative analysis of theoretical models used for modeling compound (**3**).

	N \cdots S Distance (Å)	N-C-C-S Dihedral Angle (Degrees)	Δ N \cdots S Distance (Å) [‡]	Δ N-C-C-S Dihedral Angle (Degrees) [‡]
1a (crystallographic structure data)	2.932	3,01°		
PM6	2.895	0.00°	-0.037	-3.01°
HF/6-31+G(d)	2.948	0.00°	0.016	-3.01°
HF/6-311G(d)	2.940	0.00°	0.008	-3.01°
HF/6-311+G(d,p)	2.946	0.00°	0.014	-3.01°
MP2/6-31+G(d)	2.988	22.47°	0.056	19.46°
MP2/6-311G(d)	2.933	12.83°	0.001	9.82°
MP2/6-311+G(d,p)	2.984	20.63°	0.052	17.62°
B3LYP/6-31+G(d)	2.947	0.00°	0.015	-3.01°
B3LYP/6-311G(d)	2.929	0.00°	0.003	-3.01°
B3LYP/6-311+G(d,p)	2.941	0.00°	0.009	-3.01°

[‡]The Δ -values were obtained by subtracting the calculated value from the experimental value.

1.3. Studies of structure-property relationships. These studies were made by modifying the thiophene ring of (**3**) with the introduction of electron donating and electron withdrawing groups at R₁, R₂ and R₃ positions as well as the introduction of heteroatoms in the X, Y and Z positions in the thiophene ring (**Table S3**). This series of compounds was subjected to PES scan analysis, as described before, but using only the 6-311G(d) basis set for the HF, MP2 and B3LYP levels of theory. Equilibrium geometry calculations were performed in the same way as described before.

At this point, we choose the B3LYP/6-311G(d) method as the reference for the analyses of the results in order to simplify the discussion.

The introduction of substituents at the R₁ position of thiophene ring (**Table S3**, compounds (**7**)-(13), (**28**), (**31**)) resulted in a significant ortho effect⁷ (**Figure S2**), as can be seen for data on the *anti-syn* energy differences (**Table S7**). However, as these data on the *anti-syn* energy difference were not used in our statistical correlations we decided to not exclude the data of the compounds **7-13**. Regarding the introduction of substituents on the R₂ and

R₃ positions (**Table S3**, compounds (14)-(27), (29), (30)), the energy profile was different from the initially observed for the unsubstituted compound (3), independently of the group introduced (**Figure S2**).

In general, the introduction of electron withdrawing groups tended to increase the stability of interactions 1,4-N \cdots S while electron donating groups tended to destabilize it. Data on *anti-syn* energy differences observed in the PES scan analysis for compounds (3), (7)–(31) are shown in **Table S7**.

The introduction of a nitro group in the R₂ and R₃ positions in compounds 9 and 16 (**Figure S2 B and C**), for example, resulted in increased stability of the 1,4-N \cdots S interaction. For the R₁ position, the HF and MP2 methods diverged from the observed behavior for the potential energy profile observed for the B3LYP, while the PM6 method behaved in a similar way (**Figure S2 A**), which may be related to the treatment of the electronic correlation for each method.⁸

The presence of halogens (fluorine and chlorine) at the R₁, R₂ and R₃ positions of the thiophene ring (compounds (9)-(10), (16)-(17), (23)-(24)) increased the stability of 1,4-N \cdots S interaction (**Figure S2 G-L**). However, when comparing the R₁ substitution position for the chlorine atom (**Figure S2 J**, compound (10)) is possible to note that the HF and MP2 methods moves away from the potential energy profile observed for the B3LYP method. Predicting a greater stability for the 30° conformer, but not for fluorine, this may be associated with the smaller atomic radius of fluorine atom. With the introduction of cyano (**Figure S2 D-F**, compounds (8), (15), (22)) and methoxy groups (**Figure S2 M-O**, compounds (11), (18), (25)), the changes in the potential energy profile were similar to that observed for the halogens.

The potential energy profile changes by the replacement of thiophene ring by thiazole rings, being more significant when the nitrogen atom has been introduced at X position of thiophene ring (**Figure S2 V**, (28)). This change can be related to the electronic repulsion effect of the electron lone pairs from nitrogen atoms in pyridine and thiazole rings.⁹ The same was observed for the potential energy profile when the introduction of the nitrogen atoms carried out in X and Y positions at the same time (**Figure S2 Y**, (31)).

The introduction of an amino group at the R₃ position (26) resulted in increased stability of the σ -hole N \cdots S interaction compared to (3) (**Figure S2 R**). This can be observed by concomitant increase of the interconversion energy barrier and the *anti-syn* energy difference (**Table S7**) for the B3LYP method, the others methods behaved in a similar way. The replacement at the R₂ position (19) decreased the stabilization energy initially observed for (3);

the MP2 was the unique method that diverge from the observed profile of the B3LYP method. In the case of the amino group at the R_1 position (**12**) there is also the occurrence of an intramolecular hydrogen bonding between the amino group and nitrogen atom of the pyridine ring, which results in a significant decrease in potential energy for the *anti* conformer (**Figure S2 P**). In the case of the (**12**), the subsequent equilibrium geometry calculations occurred for the 30° conformer.

The introduction of methyl group at the R_3 position (**27**) resulted in increased stability of the interaction between nitrogen and sulfur atoms for all methods, with exception of the PM6 method that predicted a decrease in the stability of the interaction compared to (**3**) (**Figure S2 U**). As for the R_2 position (**20**), no significant changes occurred in the energy profile initially observed to (**3**), but for the MP2 method it was observed an increased stabilization of the interaction between the nitrogen and sulfur atoms (**Figure S2 T**) in relation to the B3LYP method. The introduction of a methyl in R_1 position (**13**) strongly decreased the stabilization of the interaction between nitrogen and sulfur atoms as predicted by B3LYP, the other methods behaved similarly (**Figure S2 S**).

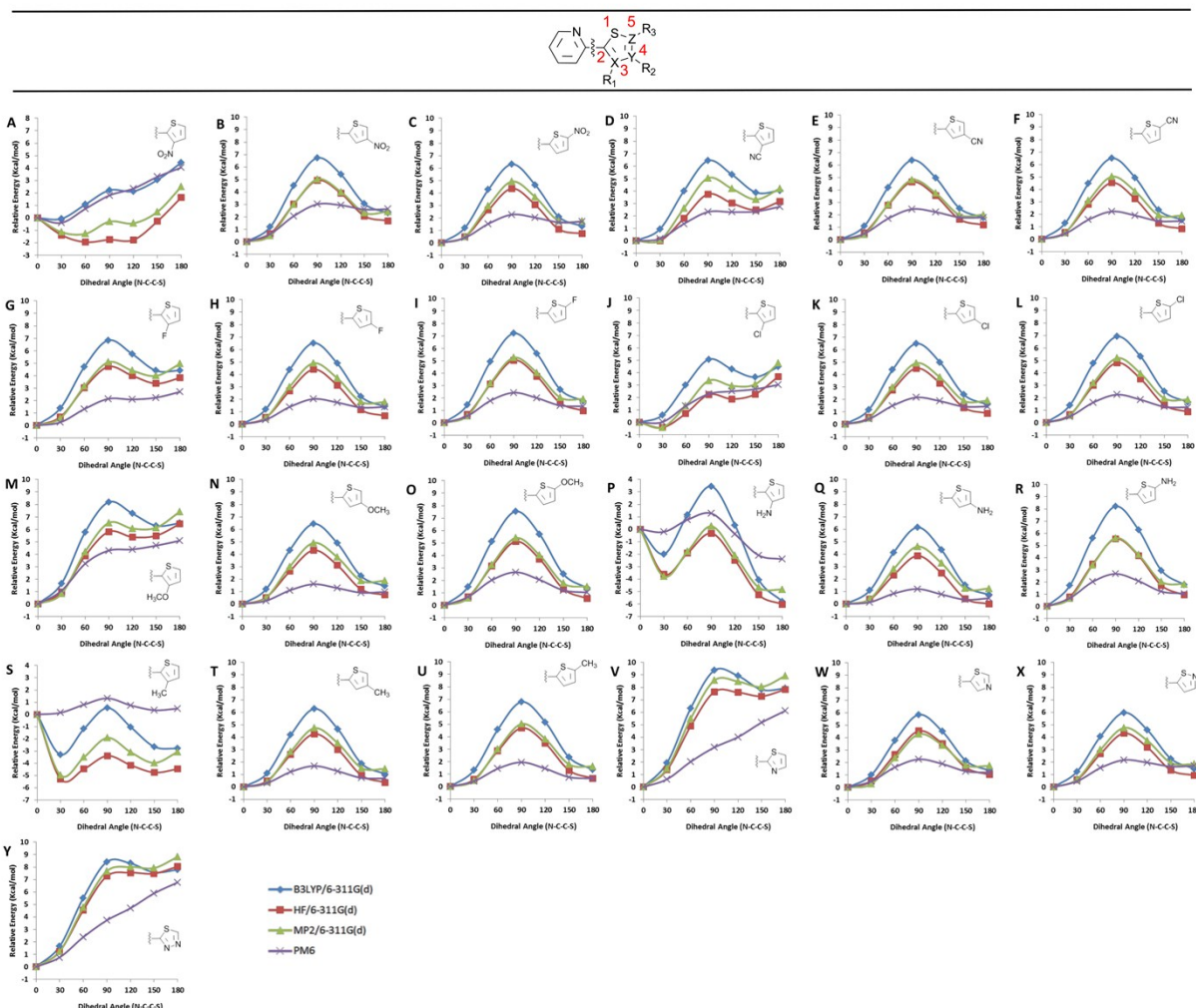
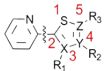
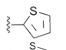
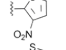
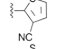
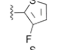
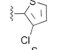
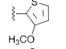
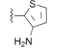
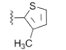
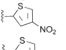
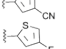
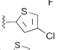
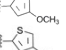
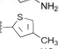
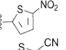
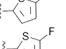
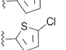
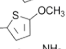
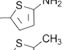
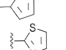
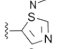
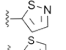
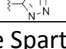






Figure S2. PES analysis for compounds (3), (7)-(31). (A) The results of the SEP analysis for (7). (B) The results of the PES analysis for (14). (C) The results of the PES analysis for (21). (D) The results of the PES analysis for (8). (E) The results of the PES analysis for (15). (F) The results of the PES analysis for (22). (G) The results of the PES analysis for (9). (H) The results of the PES analysis for (16). (I) The results of the PES analysis for (23). (J) The results of the PES analysis for (10). (K) The results of the PES analysis for (17). (L) The results of the PES analysis for (24). (M) The results of the PES analysis for (11). (N) The results of the PES analysis for (18). (O) The results of the PES analysis for (25). (P) The results of the PES analysis for (12). (Q) The results of the PES analysis for (19). (R) The results of the PES analysis for (26). (S) The results of the PES analysis for (13). (T) The results of the PES analysis for (20). (U) The results of the PES analysis for (27). (V) The results of the PES analysis for (28). (W) The results of the PES analysis for (29). (X) The results of the PES analysis for (30). (Y) The results of the PES analysis for (31). Legend: blue = B3LYP; green = MP2; red = HF; purple = PM6. All data presented here was obtained through the Spartan'14 software (Wavefunction, Inc.).

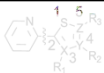
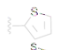
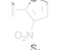
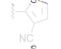
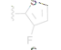
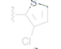
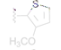
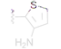
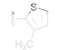
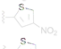
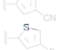
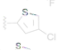

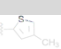
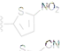
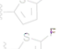
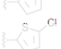
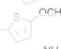
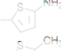

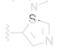
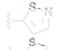
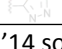
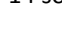



Table S3. Compounds used in the studies of structure-property relationship together with the data obtained through the B3LYP/6-311G(d) level of method.

					
Compounds		N...S Mulliken Bond Order ^a	Q _N -Q _S (Mulliken Charges) ^a	(E _{HOMO} - E _{LUMO}) ⁻¹ (eV) ^a	Lp _N →σ* _{S-C} (kcal/mol) ^b
3		0.081	-0.108	0.2174	1.05
7		0.087	-0.126	0.2500	1.28
8		0.091	-0.127	0.2326	1.50
9		0.083	-0.114	0.2174	1.11
10		0.092	-0.121	0.2174	1.67
11		0.088	-0.113	0.2326	1.27
12		0.073	-0.097	0.2326	0.77
13		0.083	-0.106	0.2174	1.17
14		0.087	-0.127	0.2326	1.20
15		0.085	-0.125	0.2174	1.16
16		0.084	-0.113	0.2273	1.14
17		0.086	-0.120	0.2273	1.29
18		0.083	-0.105	0.2326	1.09
19		0.082	-0.103	0.2500	1.10
20		0.081	-0.105	0.2222	1.07
21		0.087	-0.127	0.2564	1.30
22		0.087	-0.135	0.2381	1.36
23		0.090	-0.104	0.2326	1.48
24		0.086	-0.133	0.2326	1.43
25		0.086	-0.095	0.2381	1.22
26		0.090	-0.092	0.2500	1.22
27		0.086	-0.103	0.2273	1.22
28		0.077	-0.101	0.2174	0.90
29		0.078	-0.102	0.2128	1.10
30		0.071	-0.141	0.2083	1.09
31		0.071	-0.093	0.2000	0.87

^aData obtained through the Spartan'14 software (Wavefunction, Inc.)

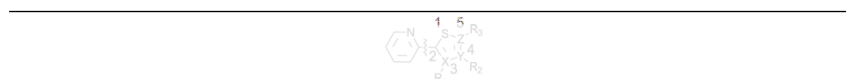
^bData obtained through the GAUSSIAN'09 package.¹⁰

Table S4. Compounds used in the studies of structure-property relationship together with the data obtained through the PM6 level of method.

				
Compounds	R	N...S Mulliken Bond Order ^a	Q _N -Q _S (Mulliken Charges) ^a	(E _{HOMO} - E _{LUMO}) ⁻¹ (eV) ^a
3		0.041	-0.144	0.0971
7		0.039	-0.157	0.0962
8		0.045	-0.173	0.0990
9		0.044	-0.152	0.0952
10		0.041	-0.149	0.0943
11		0.046	-0.151	0.1020
12		0.039	-0.130	0.0971
13		0.038	-0.132	0.0943
14		0.046	-0.172	0.0962
15		0.044	-0.171	0.0971
16		0.044	-0.152	0.0962
17		0.044	-0.166	0.1010
18		0.042	-0.138	0.0971
19		0.042	-0.139	0.1000
20		0.042	-0.141	0.0971
21		0.045	-0.177	0.1010
22		0.044	-0.187	0.1042
23		0.046	-0.146	0.1000
24		0.043	-0.184	0.1020
25		0.045	-0.127	0.099
26		0.049	-0.125	0.1010
27		0.044	-0.134	0.0980
28		0.041	-0.138	0.0943
29		0.041	-0.135	0.0950
30		0.034	-0.200	0.0926
31		0.039	-0.124	0.0901

^aData obtained through the Spartan'14 software (Wavefunction, Inc.)

Table S6. Compounds used in the studies of structure-property relationship together with the data obtained through the MP2/6-311G(d) level of method.



Compounds	R	N...S Mulliken Bond Order ^a	Q _N -Q _S (Mulliken Charges) ^a	(E _{HOMO} - E _{LUMO}) ⁻¹ (eV) ^a
3		0.062	-0.122	0.1010
7		0.048	-0.128	0.1010
8		0.077	-0.146	0.1042
9		0.072	-0.131	0.1000
10		0.066	-0.129	0.0990
11		0.075	-0.130	0.1020
12		0.062	-0.105	0.1000
13		0.059	-0.107	0.0943
14		0.073	-0.142	0.1010
15		0.073	-0.144	0.1010
16		0.073	-0.131	0.1010
17		0.073	-0.128	0.1010
18		0.072	-0.122	0.1020
19		0.070	-0.121	0.1042
20		0.067	-0.112	0.0971
21		0.076	-0.144	0.1075
22		0.074	-0.145	0.1042
23		0.075	-0.109	0.1000
24		0.072	-0.138	0.1020
25		0.073	-0.109	0.1031
26		0.074	-0.108	0.1042
27		0.073	-0.109	0.1020
28		0.068	-0.125	0.1000
29		0.065	-0.119	0.0990
30		0.058	-0.160	0.0971
31		0.062	-0.116	0.0952

^aData obtained through the Spartan'14 software (Wavefunction, Inc.)

Table S7. *Anti-syn* energy differences (kcal/mol) calculated for compounds (**3**), (**7**)–(**31**).

Compounds	Method			
	B3LYP/6-311G(d)	MP2/6-311G(d)	HF/6-311G(d)	PM6
3	1.00	1.17	0.39	0.89
7	4.44	2.51	1.65	4.05
8	4.03	4.20	3.16	2.74
9	4.42	4.95	3.82	2.70

10	4.07	4.78	3.69	3.03
11	6.49	7.41	6.43	5.09
12	-5.79	-4.84	-6.02	-2.40
13	-2.79	-3.06	-4.46	0.48
14	2.32	2.43	1.69	2.63
15	1.78	2.01	1.20	1.79
16	1.41	1.78	0.68	1.39
17	1.58	1.89	0.88	1.43
18	1.45	1.87	0.75	0.98
19	0.73	1.24	0.01	0.47
20	1.05	1.45	0.37	0.70
21	1.34	1.73	0.74	1.71
22	1.56	1.90	0.85	1.46
23	1.74	1.91	0.98	1.34
24	1.65	1.85	0.87	1.23
25	1.38	1.50	0.55	1.03
26	1.77	1.82	0.93	1.05
27	1.36	1.61	0.66	0.65
28	7.91	8.92	7.93	6.12
29	1.34	1.74	1.02	1.19
30	1.46	1.84	0.94	1.70
31	7.79	8.82	8.05	6.77

1.4. Evaluation of parameters involved in 1,4-N...S σ -hole intramolecular interactions. In order to understand the σ -hole interactions mediated by sulfur atoms in details and thereby determine the most appropriate method for the theoretical characterization of these interactions, single point calculations for the resultant geometries from

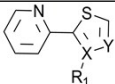
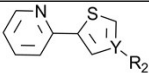
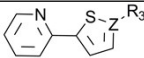
the previous step were done, maintaining the same method with the same basis set. The obtained single point calculations data were used in a simplified model of correlation using multiple linear regression analysis based on the simplified form of the Klopman-Salem equation (Equation 1) (Fleming, 2010).

$$\Delta E = \frac{Q_{Nu}Q_{El}}{\epsilon R} + \frac{2(C_{Nu}C_{El}\beta)^2}{E_{HOMO} - E_{LUMO}} \quad (\text{Eq. 1})$$

The first term (Coulomb term) of Equation 1 was represented by the product of the charges of the nitrogen and sulfur atoms. The second term (second order perturbation) was related to the inverse of the energy variation of the frontier orbitals $(E_{HOMO} - E_{LUMO})^{-1}$. The energy variation (ΔE) was considered as the Mulliken bond order between the nitrogen and sulfur atoms. The Mulliken bond orders were correlated as dependent variables, while the product of the charges of the nitrogen and sulfur atoms and the inverse of energy variation of frontier orbitals were correlated as independent variables. In other words, in our simplified model we explained the bond energy between the nitrogen and sulfur atoms through the correlation between the product of the charges of these two atoms and the inverse of the energy difference between the HOMO and LUMO.

The statistical correlations were divided into three sets: (a) compounds with groups or heteroatoms introduced at R_1 position (compounds **(3)**, **(7)**-**(13)**, **(28)** and **(31)**); (b) compounds with groups or heteroatoms introduced at R_2 position (compounds **(3)**, **(14)**-**(20)**, **(29)** and **(31)**); and (c) compounds with groups or heteroatoms introduced at R_3 position (compounds **(3)**, **(21)**-**(27)**, **(30)** and **(31)**), as described in **Table S8**.

Table S8. Data of multiple linear regression analysis about the correlation of Mulliken bond orders with the $Q_N.Q_S$ (Mulliken Charges) and the $(E_{HOMO} - E_{LUMO})^{-1}$.

						
Method	R^{2a}	Adjusted R^{2a}	R^{2b}	Adjusted R^{2b}	R^{2c}	Adjusted R^{2c}
HF/6-311G(d)	0.57679	0.45587	0.37505	0.1965	0.94974	0.93538
MP2/6-311G(d)	0.29508	0.09367	0.74724	0.67502	0.83265	0.78484

B3LYP/6-311G(d)	0.87787	0.84298	0.93275	0.91354	0.78144	0.71899
PM6	0.52729	0.39223	0.60448	0.49147	0.65704	0.55905

^aData are referred to the compounds **(3)**, **(7)-(13)**, **(28)** and **(31)**. Substitution pattern at R₁ position.

^bData are referred to the compounds **(3)**, **(14)-(20)**, **(29)** and **(31)**. Substitution pattern at R₂ position.

^cData are referred to the compounds **(3)**, **(21)-(27)**, **(30)** and **(31)**. Substitution pattern at R₃ position.

According to the coefficients of the statistical correlations, the most appropriate method for the study of theoretical characterization of σ -hole interactions based on our simplified model is B3LYP/6-311G(d). An important fact to note is that when the data for all compounds are analyzed together (without performing subdivisions in the data set), an appropriate correlation is not obtained for any method (data not shown), which could be an indication that our analysis model to explain the 1,4-N \cdots S intramolecular interactions would not be ideal.

For a more specific analysis of σ -hole interactions at the molecular orbitals level, NBO (Natural Bond Orbitals) analysis was performed with B3LYP/6-311G(d). The relationships of interactions between orbital donors and acceptors were obtained, where the orbital referred to the lone electron pair of the nitrogen atom (Lp_N) was the orbital donor and the σ^*_{S-C} orbital was the acceptor (Lp_N $\rightarrow\sigma^*_{S-C}$). The energy of interaction between these orbitals was obtained using the equation derived from the second order perturbation theory (Equation 2).¹¹

$$\Delta E_{ij} = q_i \frac{F(i,j)^2}{\varepsilon_j - \varepsilon_i} \quad (\text{Eq. 2})$$

Where q_i is the occupancy of the orbital donor, $F(i,j)$ are the elements of Fock matrix and ε_i and ε_j are the orbital energies of donors and acceptors, respectively. These data were used for a review of the statistical correlations replacing the values related to the inverse of the variation energy of the frontier orbitals (HOMO and LUMO) by the values of the interactions (Lp_N $\rightarrow\sigma^*_{S-C}$) obtained from the NBO analysis.

In this way, it was possible to obtain a good result for all compounds analyzed together **(3)**, **(7)-(31)**, with the coefficients analysis $R^2 = 0.87$ and *adjusted* $R^2 = 0.74$ for the B3LYP/6-311G(d) level of theory. These coefficients indicated that it is possible to a great extent to explain the 1,4-N \cdots S σ -hole intramolecular interactions (correlated here as Mulliken bond orders) through a direct relationship between the products of the charges of these two

atoms (nitrogen and sulfur) and the orbitals energy interactions between the lone pair of electrons of the nitrogen atom and the $\sigma^*_{\text{S-C}}$ orbital ($\text{Lp}_\text{N} \rightarrow \sigma^*_{\text{S-C}}$) obtained from NBO analysis.

1.5. Influence of adjacent groups in the σ -hole regions. The influence of adjacent groups in the σ -hole regions and the energy of the $\sigma^*_{\text{S-C}}$ orbital for a series of 3-substituted heterocyclic rings (**Figure S3**) was also analyzed. This analysis was also used to understand the modifications in the σ -hole regions in systems where there is no interaction of the sulfur atoms with these groups. The influence of the σ -hole regions was verified by equilibrium geometry calculations with subsequent implementation of single point calculations to determine the electrostatic potential maps with the B3LYP/6-311G(d) level of theory, and the energies of the $\sigma^*_{\text{S-C}}$ orbitals were also verified by the same level of theory through NBO analysis (**Figure S3**).

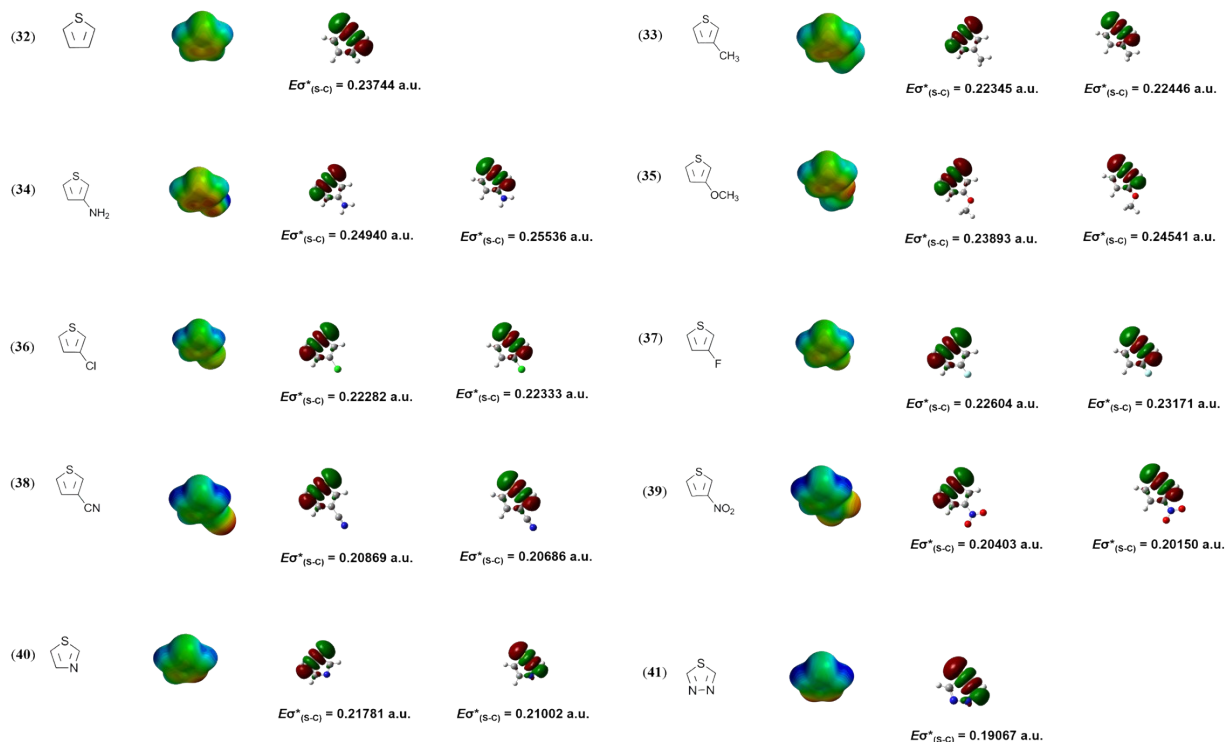


Figure S3. Electrostatic potential maps and $\sigma^*_{\text{(S-C)}}$ orbitals energy detected in NBO analysis for compounds 27-36. The scale of electrostatic potential maps is in the range of -150 to +150 kJ/mol. The energy values for the $\sigma^*_{\text{(S-C)}}$ orbitals are presented in atomic units (a.u.).

From **Figure S3**, it can be seen that the adjacent groups significantly influenced the σ -hole regions: electron withdrawing groups had a tendency to make the σ -hole regions larger, increasing the electrostatic potential of

these regions while decreasing the $\sigma^*_{\text{S-C}}$ orbitals energies, while electron donating groups had a tendency to make the σ -hole regions smaller, decreasing its electrostatic potential and increasing the $\sigma^*_{\text{S-C}}$ orbitals energies.

According to our study, 1,4-N \cdots S σ -hole intramolecular interactions are favorable interactions that can directly influence the conformational preference of compounds in where this type of intramolecular interaction is present and furthermore, these interactions are highly influenced by adjacent groups. Our data shows a good correlation with other studies in the literature,^{1,12-14} where the presence of electron withdrawing groups tended to increase the strength of interaction between the sulfur atoms and groups that can act as Lewis bases.

2. Theoretical and experimental characterization of the 1,4-N \cdots S interaction for the compounds (3) and (6).

Conformational analysis. To understand the conformational behavior of **(3)** and **(6)** (**Figure S4**), we conducted a ^1H 1D homonuclear NOESY experiments. This data are presented in **Figure S4** along with a theoretical data of PES scan analysis for **(3)** and **(6)** in DMSO through the B3LYP/6-31G(d) level of theory. Using NOESY 1D, NOE correlations are observed as oppositely phased peaks when one proton resonance is selectively irradiated. As can be seen in **Figure S4-B**, the presence of spatial correlation between the protons of the thiophene and the pyridine rings confirmed that in DMSO the nitrogen and sulfur atoms are still in a closer approximation in compound **(3)**. This was corroborated by our theoretical data that indicated a conformational stability of 1.70 kcal/mol for the *syn* conformer in comparison with the *anti* conformer for **(3)** (**Figure S4-A**), and taking in consideration the energy difference between all the conformers depicted in the PES scan analysis, we performed a Boltzmann distribution analysis that indicates the *syn* conformer had a prevalence of 90% in 298.15 K. For compound **(6)** it was not expected that this compound would have a relevant conformational stabilization since it is in the form of an oil at room temperature, a macroscopic indication that there is a lack of conformational stabilization, making packing difficult. The NOESY 1D analysis corroborated these observations since, through the selective irradiation of H3, it was possible to identify both correlations with the conformer *syn* and *anti* of **(6)** (**Figure S4**). This was also corroborated by our theoretical conformational analysis, which indicated a small energy difference between these two conformers ($\Delta E_{\text{anti-syn}} = -0.03$ kcal/mol) and each conformer represents approximately 35% of the conformers according to Boltzmann's distribution analyzes at 298.15 K.

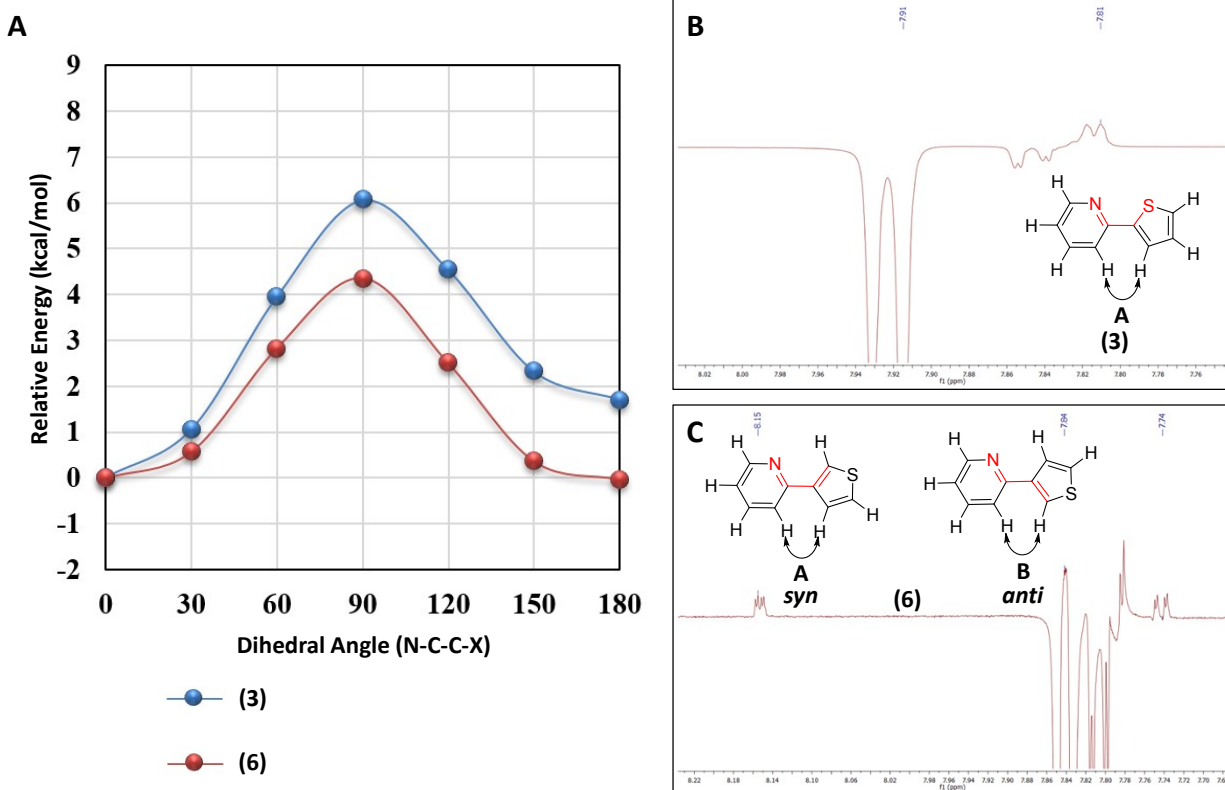


Figure S4. Conformational analysis and data from ^1H 1D homonuclear NOESY experiments of compounds **(3)** and **(6)**. (A) PES scan of the dihedral angles marked in red in the compounds **(3)** and **(6)** through the B3LYP/6-31G(d) level of method in DMSO (SM8 solvent model). (B) 1D NOESY spectrum of compound **(3)**, irradiation was conducted at 7.91 ppm (H3) and correlation was observed with H3' (7.81 ppm) indicated by the **A** arrow (H3 – H3'). (C) 1D NOESY spectrum of compound **(6)**, irradiation was conducted at 7.83 ppm (H3) and correlations observed with H4' (8.15 ppm) and H2' (7.76 ppm) are indicated by the arrows **A** (H4' – H3) and **B** (H2' – H3).

Vibrational spectra. We conducted a careful analysis of the vibrational spectra of compounds **(3)** and **(6)** and compared it to our theoretical ones. We obtained a good correlation between our theoretical and experimental spectra (**Tables S9** and **S10**). Added to this, we performed a total energy distribution analysis (TED) through VEDA4 software,¹⁵ which allowed us to point the vibrational modes related to each frequency in the experimental and theoretical spectra (**Tables S9** and **S10**). We also compared our results to the published vibrational correlation of compound **(3)**.² In this way, we highlighted the main region of the vibrational spectra for these two compounds in **Figure S5** (1800–600 cm^{-1}). In a general way, it is clear that there are significant differences between the

vibrational profile of **(3)** and **(6)**. Besides that, in a more specifically way we tried to analyze the main regions of the CS and CN bonds stretching frequencies aiming to compare the bond strength of these groups in these two compounds. According to our results, the CN stretching wavenumbers emerge in the interval of 1600–1200 cm^{-1} and appears to have no significant differences in the CN bond strength in compounds **(3)** and **(6)**. On the other hand, analyzing the specific modes of CS stretching there appears to be differences in the CS bond strength in each system. For **(3)** these modes occurred in regions ranging from 738 to 853 cm^{-1} in the IR spectra and from 749 to 853 cm^{-1} in the Raman spectra, while for **(6)** these vibration modes appeared in the region between 815 and 862 cm^{-1} in the IR spectra and 822 cm^{-1} in the Raman spectra. According to this, the CS bond strength of **(3)** seems to be weaker in relation to **(6)**, which can be a direct consequence of the donation of the electron pair of the nitrogen atom to the σ^* C-S orbital. All of our theoretical and experimental data together strongly suggest an occurrence of an intramolecular interaction between the nitrogen and sulfur atoms in the compound **(3)**.

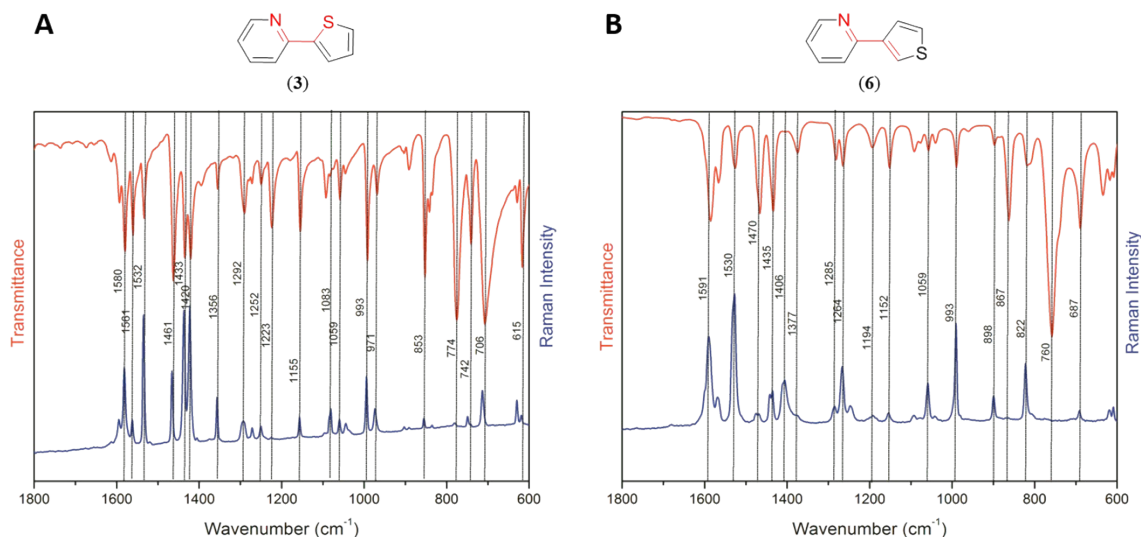
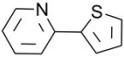


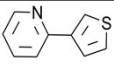
Figure S5. Data from IR (red) and Raman (blue) spectroscopy. (A) Data obtained for the compound **(3)**. (B) Data obtained for the compound **(6)**.

Table S9. Experimental and calculated vibrational wavenumbers (cm^{-1}) related with the vibrational modes of nitrogen and sulfur atoms of compound (**3**).

				
Mode	TED(%) > 10%	Experimental		B3LYP/6-311G(d)
		IR	Raman	Freq.
1	τNCCC (16) + γCCNC (27)	-	-	104
2	δCCN (37)	-	-	140
3	τNCCC (28)	-	260	246
4	δCNC (25)	-	324	321
5	δCCN (32) + δSCC (13)	-	-	408
6	τHCNC (12) + τNCCC (20) + τCNCC (13)	-	-	412
7	τSCCC (53) + γCCNC (12)	-	-	452
8	τSCCC (21) + γCCNC (19)	-	-	544
9	δNCC (22) + δSCC (11)	628	630	632
10	νSC (12) + δNCC (10) + δSCC (41)	-	-	641
11	τHCCS (26) + τHCSC (67)	706	713	704
12	δSCC (20)	-	-	725
13	νSC (38) + δSCC (39)	738	749	748
14	τHCCN (24) + τNCCC (10) + τCNCC (27)	-	-	750
15	τHCCN (14) + τCNCC (17) + γCCNC (19)	775	780	789
16	τHCSC (13)	836	836	831
17	νSC (34) + δHCS (10)	853	853	861
18	τHCCN (27)	892	891	886
19	τHCCS (51) + τHCSC (12) + τSCCC (10)	-	-	898
20	τHCNC (52) + τCNCC (12)	-	-	972
21	τHCCN (25) + τHCNC (16)	967	974	993
22	δNCC (15) + δNCC (50)	991	997	1010
23	νCC (17) + δHCS (36)	1093	1083	1112
24	νNC (11)	1223	1249	1247
25	νNC (43)	1273	1272	1292
26	νNC (16)	1292	1294	1307
27	νNC (21)	-	-	1322
28	δHCS (23)	1354	1357	1396
29	νNC (18) + δHCN (28)	1462	1466	1505
30	νNC (15)	1560	1561	1610
Linear correlation coefficients (R^2)		0.999542	0.999597	

ν : stretching. δ : bending. τ : torsion. γ : out of plane bending

Table S10. Experimental and calculated vibrational wavenumbers (cm^{-1}) related with the vibrational modes of nitrogen and sulfur atoms of compound (**6**).

				
Mode	TED(%) > 10%	Experimental		B3LYP/6-311G(d)
		IR	Raman	Freq.
1	γCCNC (29) + τSCCC (28) + τNCCC (18)	-	-	98
2	δCCN (38)	-	-	157
3	τSCCC (36) + τNCCC (30)	-	-	246
4	δCNC (14) + δCCC (11)	-	-	324
5	τCNCC (19) + τNCCC (16) + τHCNC (10)	-	-	413
6	δCCN (34) + δCNC (12)	-	-	432
7	τSCCC (19)	-	-	452
8	γCCNC (29)	-	-	506
9	νSC (18) + δSCC (63)	-	609	627
10	δNCC (33) + δCNC (19) + δCCC (28)	634	618	636
11	τHCCS (12)	-	-	642
12	τHCSC (90)	-	-	677
13	τCNCC (27) + τNCCC (13) + τHCCN (16)	-	-	749
14	τHCSC (49) + τHCCN (17)	760	-	768
15	νSC (13)	815	822	815
16	γCCNC (29) + τCNCC (15)	-	-	820
17	νSC (48)	862	-	870
18	τHCCN (28)	-	-	889
19	τHCSC (17) + τHCCS (70) + δSCC (16)	896	900	915
20	τCNCC (11) + τHCNC (50)	-	-	972
21	τHCNC (17) + τHCCN (25)	-	-	993
22	δNCC (17)	989	991	1010
23	δCNC (12)	1040	-	1061
24	δHCS (13)	1057	1062	1082
25	δHCS (40)	1091	-	1109
26	δHCS (50)	1195	1192	1230
27	νNC (35)	-	1247	1283
28	νNC (15)	1264	1268	1298
29	δHCN (31) + νNC (29)	1282	1285	1320
30	δHCN (27) + νNC (17)	1465	1471	1510
31	νNC (17)	1565	1568	1613
Linear correlation coefficients (R^2)		0.999889	0.999787	

ν : stretching. δ : bending. τ : torsion. γ : out of plane bending

UV spectra. The UV spectra of **(3)** and **(6)** are presented in **Figure S6**. As can be seen, **(3)** had a bathochromic shift in comparison with **(6)**. Added to this, we also observed the orbital energy differences of the HOMO (sulfur lone pair – Lp(S)) in both systems, because with an electron density inserted by the iminic nitrogen into the sulfur atom, an increase in Lp(S) orbital energy would be observed in comparison with the negative control (Lp(S) of **(6)**). These theoretical analyzes were corroborated by our UV experimental data, highlighting the $\Delta E(\text{HOMO-LUMO})$ difference of both systems, which is in agreement with our theoretical data.

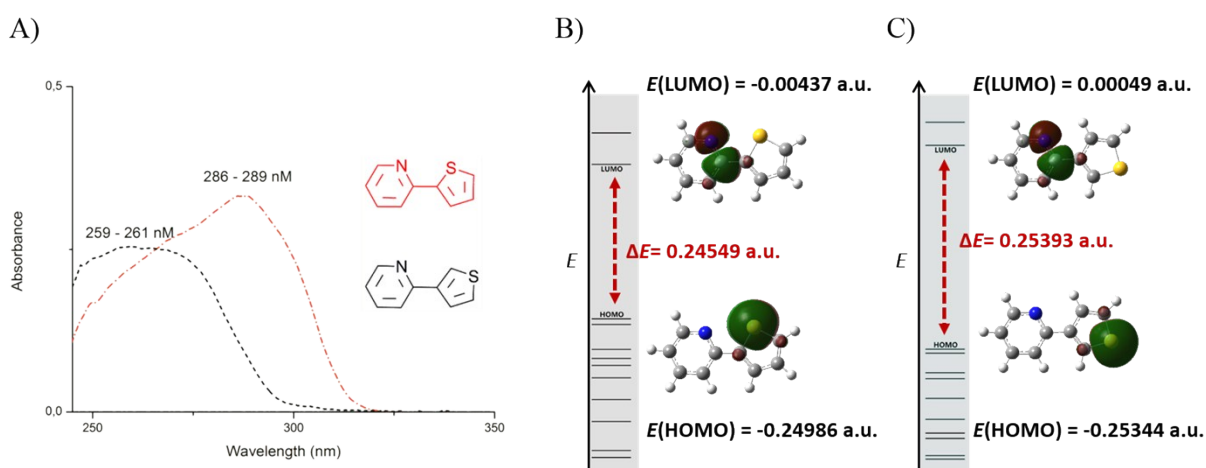


Figure S6. HOMO-LUMO energy difference in **(3)** and **(6)**. A) Experimental UV spectra of **(3)** (red dashes) and **(6)** (black dashes). B) NBO analysis of the $\Delta E(\text{HOMO-LUMO})$ for **(3)** ($\Delta E=0.24549 \text{ a.u.}$) through the B3LYP/6-311G(d) method. C) NBO analysis of the $\Delta E(\text{HOMO-LUMO})$ for **(6)** ($\Delta E=0.25393 \text{ a.u.}$) through the B3LYP/6-311G(d) method.

Charges and ^{15}N chemical shifts. In the same way as previously observed for **LASSBio-294 (1)** and **LASSBio-897 (2)**, the sulfur atom behaves like an electrophile in both **(3)** and **(6)**, having a more positive charge in **(3)**. Our theoretical data also showed that the pyridinic nitrogen behaves like a nucleophile in both systems, being in **(3)** more nucleophilic than **(6)**, which were confirmed by (^1H - ^{15}N) HMBC spectra (**Table S11**).

Table S11. Data about nitrogens and sulfur Mulliken charges and ^{15}N chemical shifts for compounds **(3)** and **(6)**.

Mulliken charges were obtained through the B3LYP/6-311G(d) method.

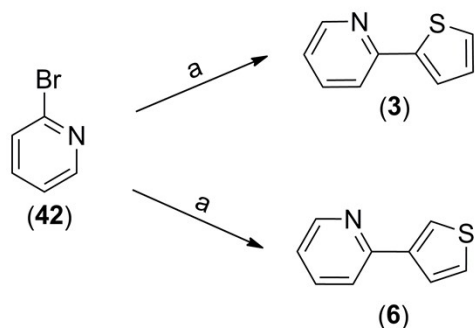
Compounds	Pyridinic N Mulliken charges	S Mulliken charges	Pyridinic ^{15}N chemical shift (ppm)
(3)	-0.339	0.319	-77.7
(6)	-0.329	0.297	-74.3

Chemistry. The compounds (**3**) and (**6**) were synthesized according to the procedures depicted in **Scheme 1^a**.¹⁶ The synthesis was carried out by a Suzuki coupling under microwave irradiation of (**42**) with 2-thienylboronic acid and 3-thienylboronic acid, generating (**3**) and (**6**) in 91% and 92% yield, respectively.

2-(thiophen-2-yl)pyridine (3). mp 61 °C. ¹H NMR (500 MHz): δ 8.52 (1H, d, *J* = 4.5 Hz), δ 7.91 (1H, d, *J* = 8.0 Hz), δ 7.83 (1H, ddd, *J* = 8.0, 7.6, 1.2 Hz), δ 7.80 (1H, d, *J* = 4.0 Hz), δ 7.63 (1H, d, *J* = 5.0 Hz), δ 7.27 (1H, dd, *J* = 7.6, 1.2 Hz), δ 7.16 (1H, dd, *J* = 5.0, 4.0 Hz). LRMS calculated for C₉H₇NS: [M]⁺ = 161.03. Found: [M + H]⁺ = 161.89. 97.9 % purity in HPLC, *t_r* = 4.17 min (λ = 254 nm).

2-(thiophen-3-yl)pyridine (6). ¹H NMR (500 MHz): δ 8.60 (1H, d, *J* = 4.8 Hz), δ 8.20 (1H, d, *J* = 2.0 Hz), δ 7.88 (1H, d, *J* = 8.0 Hz), δ 7.83 (1H, td, *J* = 8.0, 7.4, 1.4 Hz), δ 7.78 (1H, dd, *J* = 5.0, 1.0 Hz), δ 7.66 (1H, dd, *J* = 5.0, 2.0 Hz), δ 7.28 (1H, ddd, *J* = 7.4, 4.8, 1.1 Hz). LRMS calculated for C₉H₇NS: [M]⁺ = 161.03. Found: [M + H]⁺ = 161.88. 99.7 % purity in HPLC, *t_r* = 4.03 min (λ = 254 nm).

Scheme 1^a.



^aReagents and Conditions: (a) thiophen-2-ylboronic acid or thiophen-3-ylboronic acid, Na₂CO₃, PdCl₂(PPh₃)₂, H₂O, 2-propanol, (80°C and 40 min), 91-92%.

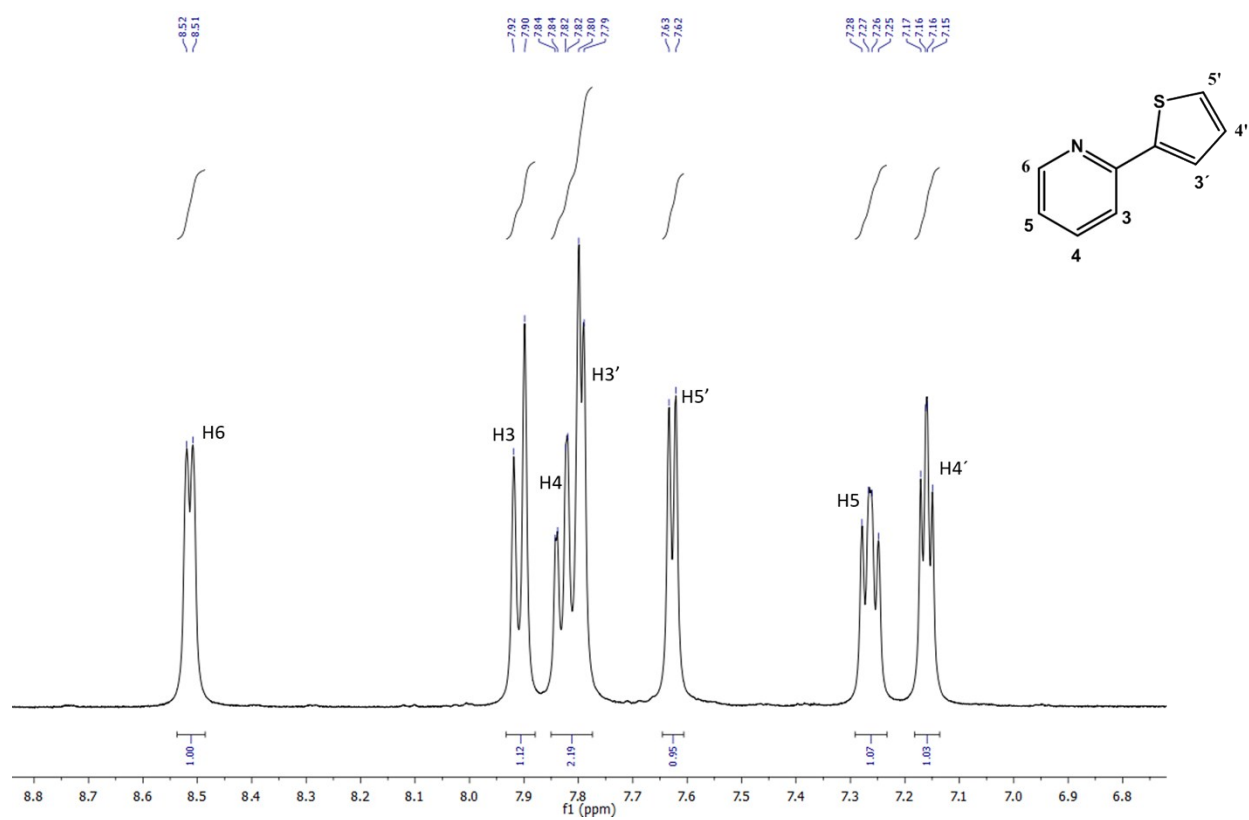


Figure S7. ^1H -NMR spectra of compound (3), 500 MHz, $\text{DMSO}-d_6$.

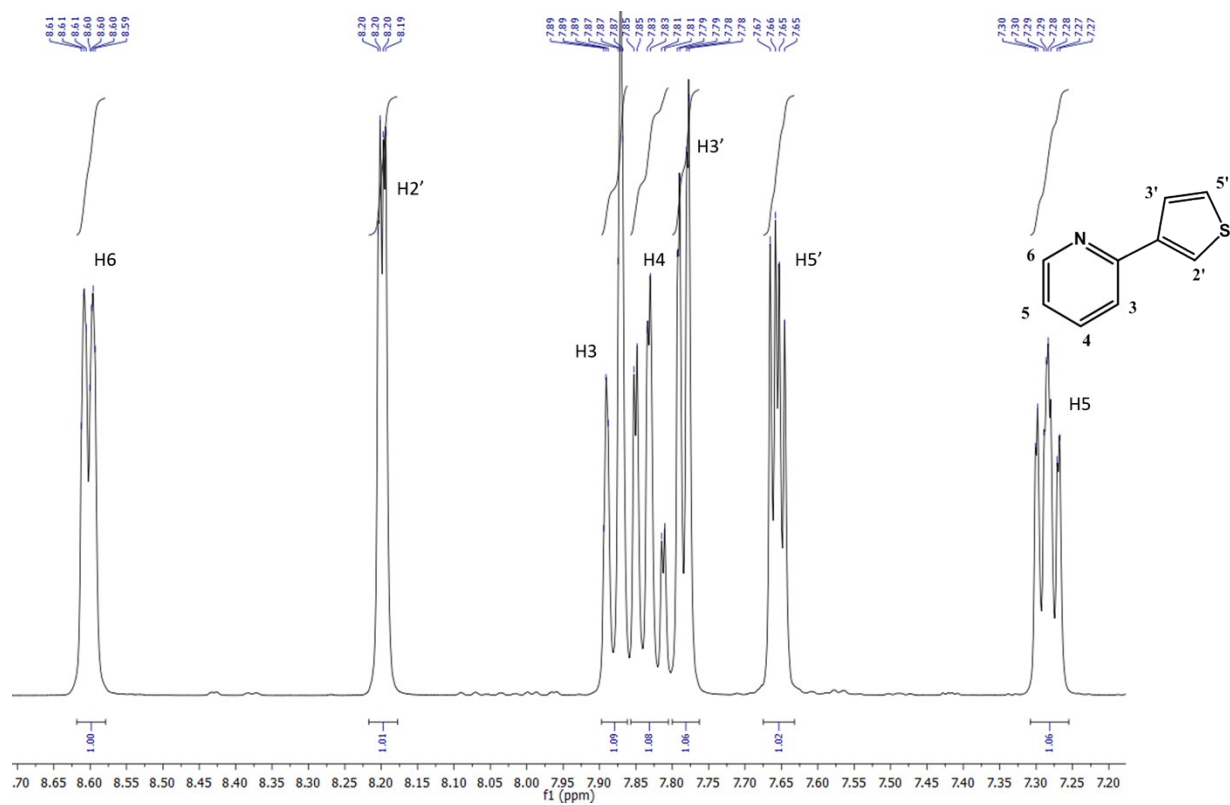


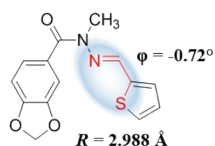
Figure S8. ^1H -NMR spectra of compound (6), 500 MHz, $\text{DMSO}-d_6$.

3. Theoretical and experimental characterization of the 1,4-N \cdots S interaction for the compounds LASSBio-785 (4) and LASSBio-1289 (5).

Conformational analysis.

A)

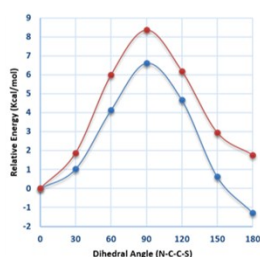
LASSBio-785 (4) Crystallographic Structure



LASSBio-1289 (5) Crystallographic Structure



B)



— LASSBio-785

$E(\text{anti-syn}) = 1.77 \text{ Kcal/mol}$

— LASSBio-1289

$E(\text{anti-syn}) = -1.28 \text{ Kcal/mol}$

C)

LASSBio-785 (4) Theoretical Conformation

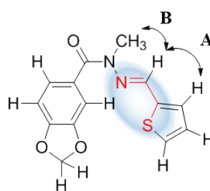


LASSBio-1289 (5) Theoretical Conformation



D)

LASSBio-785 (4) NOESY results



E)

LASSBio-1289 (5) NOESY results

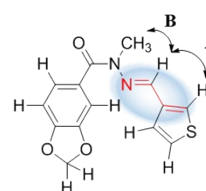


Figure S9. Conformational analysis of **LASSBio-785 (4)** and **LASSBio-1289 (5)**. A) Data of the crystallographic structures of **LASSBio-785 (4)** and **LASSBio-1289 (5)**. B) PES scan analysis of the N-C-C-X dihedral angle (thiophene conformation) obtained through B3LYP/6-31G(d) method in DMSO solvent model (SM8) available in Spartan'14. C) Final theoretical conformation obtained through equilibrium geometry calculations of the lower energy conformer observed in (B) with B3LYP/6-311G(d) method. D) Observed ^1H spatial interactions for **LASSBio-785 (4)** in the ^1H 2D homonuclear NOESY experiment (**A** = δ 8.18, 7.35; **B** = δ 8.18, 3.41). E) Observed ^1H spatial interactions for **LASSBio-1289 (5)** in the ^1H 2D homonuclear NOESY experiment (**A** = δ 8.00, 7.14; **B** = δ 8.00, 3.39).

Vibrational spectra.

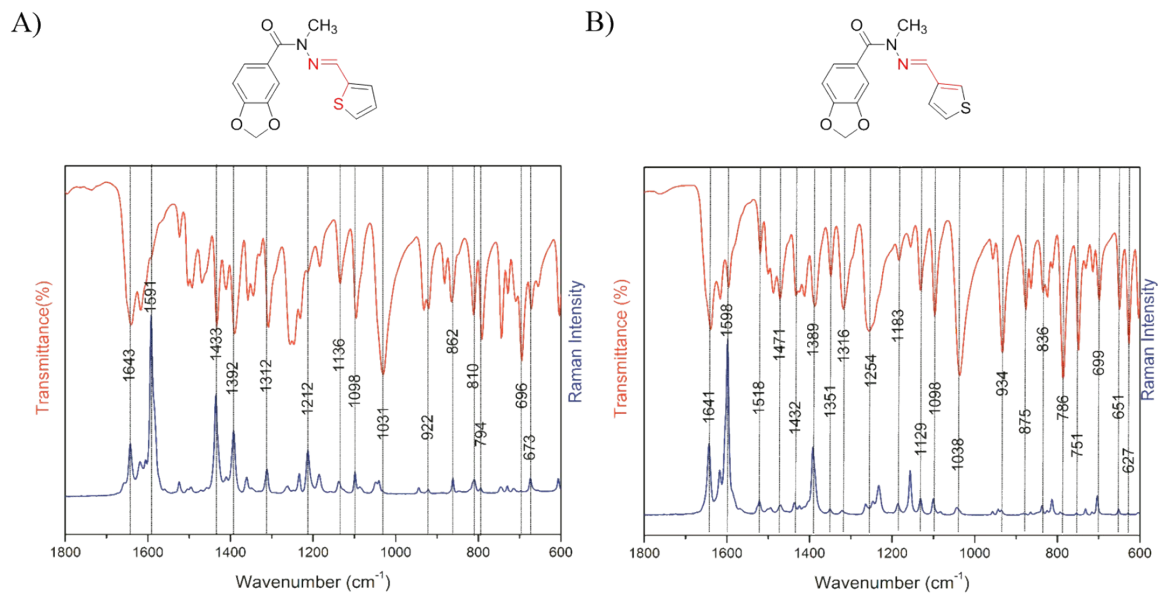
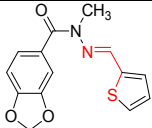


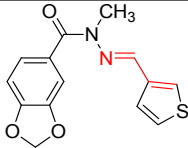
Figure S10. Data from IR (red) and Raman (blue) spectroscopy. (A) Data obtained for the **LASSBio-785 (4)**. (B) Data obtained for the compound **LASSBio-1289 (5)**.

Table S12. Experimental and calculated vibrational wavenumbers (cm^{-1}) related with the vibrational modes of nitrogen and sulfur atoms of compound **LASSBio-785 (4)**.

				
Mode	TED(%) > 10%	Experimental		B3LYP/6-311G(d)
		IR	Raman	Freq.
1	$\tau\text{CCNN (10)} + \tau\text{NNCC (36)}$	-	-	26
2	$\delta\text{CCN (10)} + \delta\text{NNC (10)}$	-	-	30
3	$\tau\text{CNNC (31)} + \tau\text{CCCN (32)}$	-	-	35
4	$\tau\text{CCCN (11)}$	-	-	68
5	$\tau\text{CCNN (25)} + \gamma\text{CCNN (20)}$	-	-	96
6	$\delta\text{CCN (10)}$	-	-	101
7	$\tau\text{CNNC (17)} + \tau\text{CCCN (16)} + \tau\text{NNCC (13)}$	-	-	132
8	$\delta\text{NNC (11)} + \gamma\text{CCNN (10)}$	-	-	179
9	$\delta\text{NNC (10)}$	-	-	215
10	$\gamma\text{CCNN (11)}$	-	-	246
11	$\delta\text{CNN (23)}$	-	-	268
12	$\tau\text{CNNC (21)} + \tau\text{CCCN (10)}$	-	-	317
13	$\tau\text{CCNN (36)} + \tau\text{SCCC (19)} + \gamma\text{CCNN (21)}$	-	-	362
14	$\delta\text{CNN (17)}$	-	-	407
15	$\delta\text{CNN (17)}$	-	-	423
16	$\delta\text{CNN (15)}$	-	-	458
17	$\tau\text{CCNN (11)} + \tau\text{SCCC (48)}$	-	-	513
18	$\delta\text{NNC (16)}$	-	-	549
19	$\tau\text{SCCC (14)}$	-	-	586
20	$\nu\text{SC (10)} + \delta\text{SCC (24)}$	-	-	614
21	$\delta\text{SCC (27)}$	-	-	679
22	$\tau\text{HCCS (24)} + \tau\text{HCSC (69)}$	696	-	702
23	$\nu\text{SC (18)}$	-	-	735
24	$\nu\text{SC (15)}$	-	-	750
25	$\nu\text{SC (13)} + \delta\text{CNN (16)} + \delta\text{CCN (13)}$	743	-	799
26	$\tau\text{HCCS (11)} + \tau\text{HCSC (13)}$	-	-	821
27	$\nu\text{SC (22)} + \delta\text{SCC (13)}$	-	-	868
28	$\tau\text{HCCS (56)} + \tau\text{HCSC (14)} + \tau\text{SCCC (12)}$	-	-	897
29	$\tau\text{HCNN (86)}$	882	-	927
30	$\nu\text{NN (12)}$	1030	-	1057
31	$\delta\text{HCS (46)}$	-	-	1110
32	$\nu\text{NN (12)}$	1231	1234	1277
33	$\nu\text{NN (13)}$	1251	-	1292
34	$\delta\text{HCN (29)}$	1308	1311	1335
35	$\delta\text{HCS (11)}$	1357	1360	1383
36	$\delta\text{HCN (28)}$	1388	1392	1416
37	$\nu\text{NC (60)} + \delta\text{HCN (11)}$	-	1591	1653
Linear correlation coefficients (R^2)		0.998454	0.995362	

ν : stretching. δ : bending. τ : torsion. γ : out of plane bending

Table S13. Experimental and calculated vibrational wavenumbers (cm^{-1}) related with the vibrational modes of nitrogen and sulfur atoms of compound **LASSBio-1289 (5)**.

				
Mode	TED(%) > 10%	Experimental		B3LYP/6-311G(d)
		IR	Raman	Freq.
1	τNNCC (26)	-	-	27
2	δCNN (11) + δCCN (11) + τNNCC (13)	-	-	30
3	τCNNC (29) + τCCCN (44)	-	-	36
4	τCCCN (10)	-	-	67
5	τCCNN (20) + τNNCC (11) + τSCCC (12) + γCCNN (14)	-	-	95
6	δCCN (11)	-	-	109
7	τCNNC (18) + τNNCC (11) + τSCCC (10)	-	-	131
8	γCCNN (13)	-	-	182
9	δNNC (13)	-	-	216
10	τSCCC (14) + γCCNN (13)	-	-	247
11	δCCN (24) + δCCN (13)	-	-	264
12	τCNNC (16) + τCCCN (10)	-	-	315
13	τCCNN (40) + τSCCC (32) + γCCNN (18)	-	-	379
14	δCCN (22)	-	-	403
15	δCCN (17)	-	-	422
16	δCCN (10)	-	-	463
17	δNNC (14)	-	-	558
18	νSC (13) + δSCC (12)	-	-	602
19	δSCC (29)	-	-	612
20	τHCCS (18)	627	-	639
21	δSCC (14)	651	-	661
22	τHCSC (86)	-	-	682
23	τHCSC (69)	-	-	778
24	δCCN (11)	786	-	799
25	νSC (57) + δHCS (11)	824	-	867
26	τHCCS (59) + τHCSC (20)	-	-	900
27	τHCNN (89)	-	-	938
28	νNN (12)	1036	1038	1059
29	δHCS (35)	-	-	1107
30	δHCS (55)	-	-	1189
31	νNN (12) + δHCS (16)	1182	1182	1264
32	νNN (10)	1254	-	1289
33	δHCN (24)	1316	-	1337
34	δHCN (35)	1389	1392	1408
35	νNC (59) + δHCN (11)	1598	1598	1659
Linear correlation coefficients (R^2)		0.998229	0.992238	

ν : stretching. δ : bending. τ : torsion. γ : out of plane bending

UV spectra.

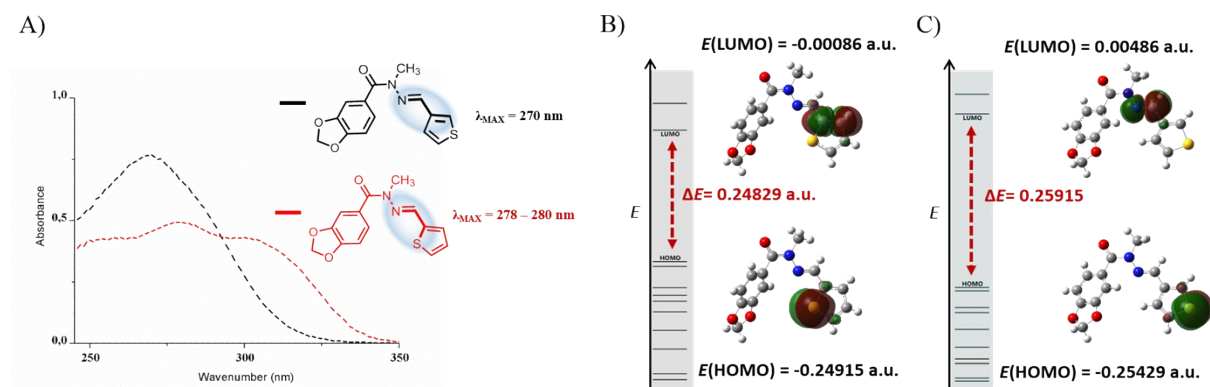


Figure S11. HOMO-LUMO energy difference in **LASSBio-785 (4)** and **LASSBio-1289 (5)**. A) Experimental UV spectra of **LASSBio-785 (4)** (red dashes) and **LASSBio-1289 (5)** (black dashes). B) NBO analysis of the $\Delta E(\text{HOMO-LUMO})$ for **LASSBio-785 (4)** ($\Delta E = 0.24829$ a.u.) through the B3LYP/6-311G(d) method. C) NBO analysis of the $\Delta E(\text{HOMO-LUMO})$ for **LASSBio-1289 (5)** ($\Delta E = 0.25915$ a.u.) through the B3LYP/6-311G(d) method.

Charges and ^{15}N chemical shifts.

Table S14. Data about the nitrogens and sulfur Mulliken charges and ^{15}N chemical shifts for the compounds **LASSBio-785 (4)** and **LASSBio-1289 (5)**. Mulliken charges were obtained through the B3LYP/6-311G(d) method.

	Iminic N Mulliken charges	Amidic N Mulliken charges	S Mulliken charges	Iminic ^{15}N chemical shift (ppm)	Amidic ^{15}N chemical shift (ppm)
LASSBio-785 (4)	-0.210	-0.261	0.317	-59.2	-211.5
LASSBio-1289 (5)	-0.200	-0.261	0.300	-55.0	-211.8

Chemistry. LASSBio-785 (4) and LASSBio-1289 (5) were synthesized according to the proceedings described in Kümmerle, *et al* (2009).¹⁷

N-Methyl (2-thienylidene)3,4-methylenedioxybenzoylhydrazine (LASSBio-785). mp 141 °C. ¹H NMR data are in agreement with those previously published.¹⁸ ¹³C NMR: δ 29.2, 103.9, 107.6, 110.7, 125.7, 128.2, 128.4, 128.5, 130.4, 135.9, 140.3, 146.5, 149.2, 168.6. LRMS calculated for C₁₄H₁₂N₂O₃S: [M]⁺ = 288.06. Found: [M + H]⁺ = 289.14. 99.3% purity in HPLC, t_r = 6.80 min (λ = 254 nm).

N-Methyl (3-thienylidene)3,4-methylenedioxybenzoylhydrazine (LASSBio-1289). mp 147 °C. ¹H NMR data are in agreement with those previously published.¹⁹ ¹³C NMR: δ 29.2, 101.9, 107.7, 110.5, 124.7, 125.1, 127.6, 127.8, 129.0, 136.4, 138.5, 146.7, 149.2, 169.0. LRMS calculated for C₁₄H₁₂N₂O₃S: [M]⁺ = 288.06. Found: [M + H]⁺ = 289.13. 98.9% purity in HPLC, t_r = 7.07 min (λ = 254 nm).

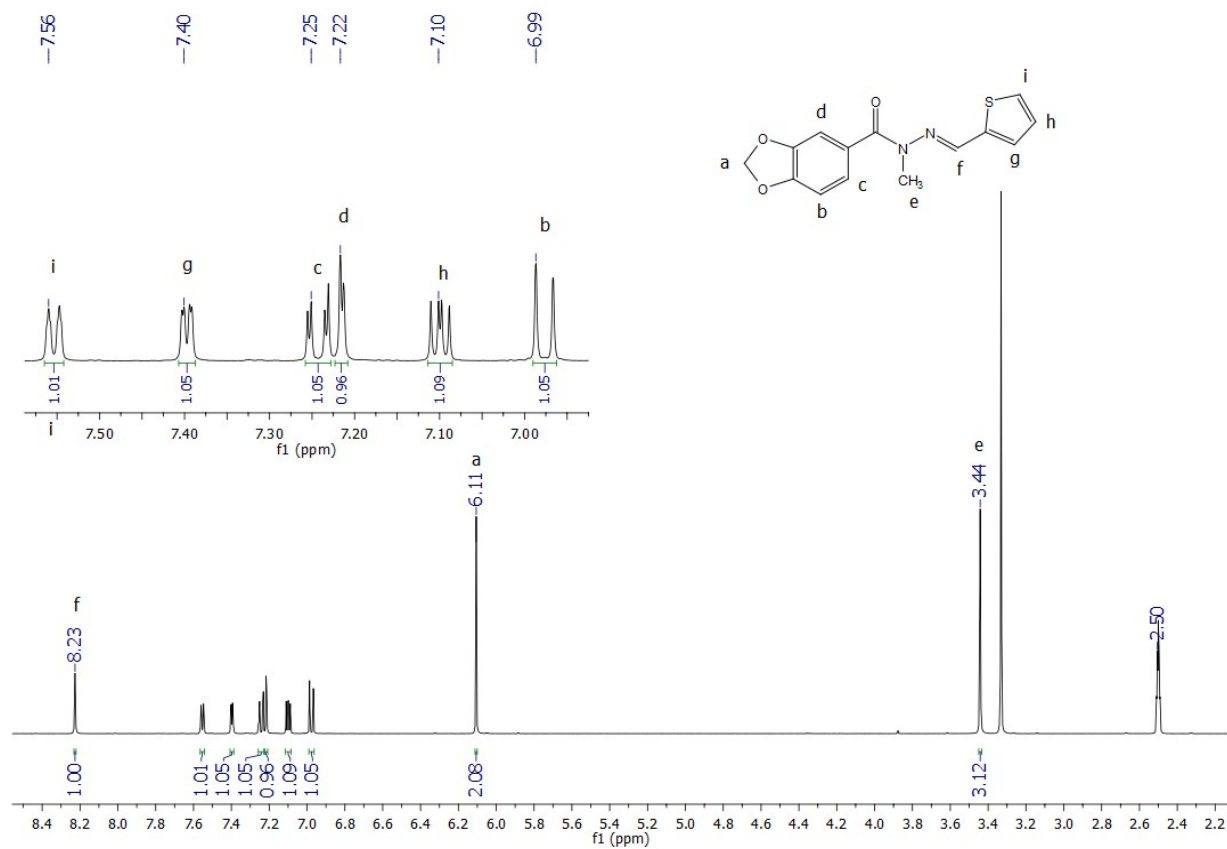


Figure S12. ^1H -NMR spectra of compound **LASSBio-785 (4)**, 400 MHz, $\text{DMSO}-d_6$.

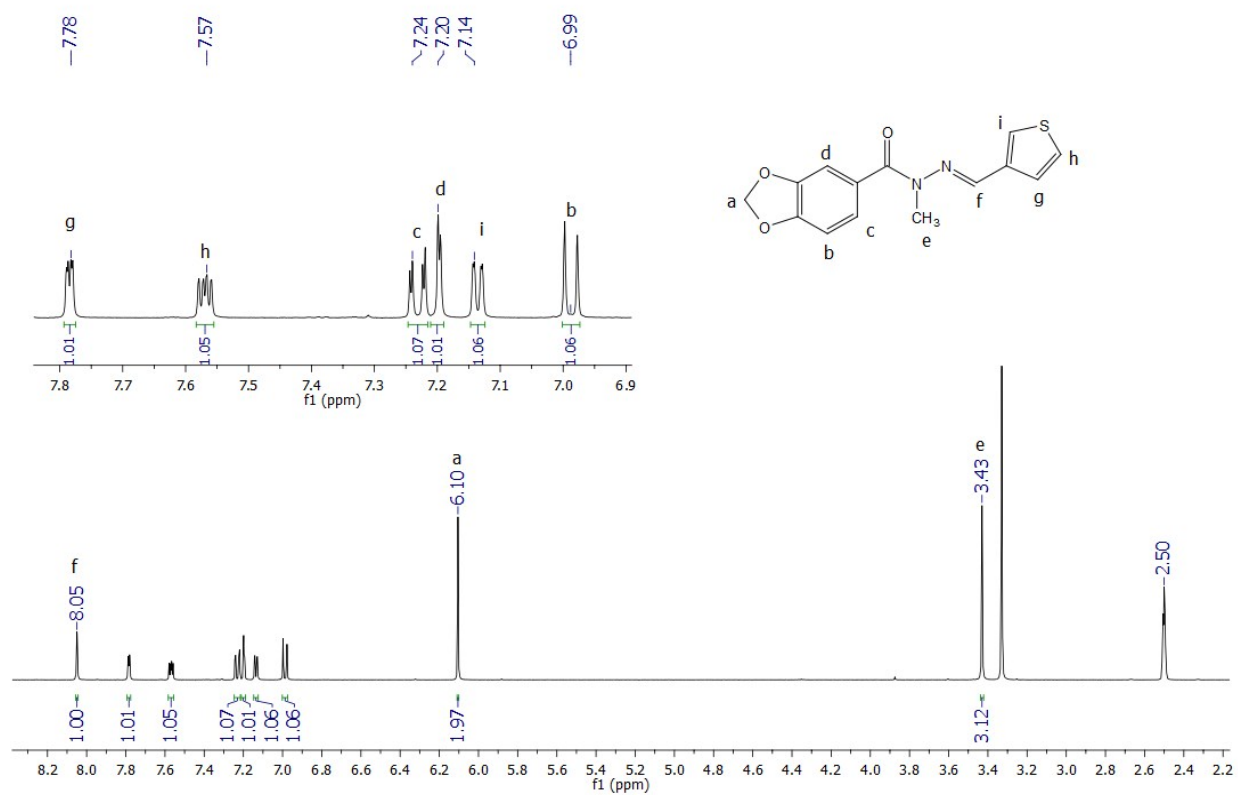
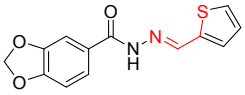


Figure S13. ^1H -NMR spectra of compound **LASSBio-1289 (5)**, 400 MHz, $\text{DMSO-}d_6$.

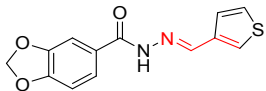
4. Additional information for the characterization of LASSBio-294 (1) and LASSBio-897 (2).

Table S15. Experimental and calculated vibrational wavenumbers (cm^{-1}) related with the vibrational modes of nitrogen and sulfur atoms of compound **LASSBio-294 (1)**.

				
Mode	TED(%) > 10%	Experimental		B3LYP/6-311G(d)
		IR	Raman	Freq.
1	τCCCN (16) + τCCNN (18) + τNNCC (37)	-	-	25
2	τCNNC (25) + τNNCC (14)	-	-	32
3	δCCN (12) + δCNN (16) + δNNC (22)	-	-	38
4	τCNNC (11) + τCCCN (25)	-	-	67
5	δCCN (14)	-	-	94
6	τCCNN (11)	-	-	121
7	τCNNC (29) + τCCCN (19)	-	-	153
8	δNNC (17)	-	-	238
9	τCCCN (12) + τNNCC (18)	-	-	259
10	τCCNN (24) + τSCCC (14)	-	-	347
11	δCCN (11)	-	-	448
12	τSCCC (15)	-	-	507
13	τSCCC (42)	-	-	512
14	τHNNC (74)	-	-	523
15	τSCCC (13)	-	-	584
16	νSC (15) + δSCC (49)	-	-	665
17	δCCN (11)	-	-	688
18	τHCSC (66)	680	-	705
19	νSC (36)	758	-	764
20	τHCSC (14)	811	-	821
21	νSC (18)	844	-	863
22	τHCSC (15)	-	-	897
23	τHCNN (87)	-	-	942
24	δHCS (46)	1096	-	1111
25	νNN (23)	1115	1119	1149
26	νNN (10)	-	-	1153
27	νNN (17)	1166	1169	1182
28	δHCS (14) + δHCN (43)	-	-	1354
29	δHCS (14) + δHCN (20)	-	-	1405
30	δHNN (36)	-	1516	1556
31	δHNN (30)	1555	1567	1586
32	νNC (69) + δHCN (10)	1592	1592	1672
Linear correlation coefficients (R^2)		0.999007	0.995831	

ν : stretching. δ : bending. τ : torsion. γ : out of plane bending

Table S16. Experimental and calculated vibrational wavenumbers (cm^{-1}) related with the vibrational modes of nitrogen and sulfur atoms of compound **LASSBio-897 (2)**.

				
Mode	TED(%) > 10%	Experimental		B3LYP/6-311G(d)
		IR	Raman	Freq.
1	τCCNN (19) + τNNCC (48)	-	-	28
2	τCNNC (21) + τCCCN (20) + τNCCC (32)	-	-	34
3	δCNN (16) + δCCN (10) + δNNC (19)	-	-	37
4	τCCCN (26) + τNCCC (40)	-	-	66
5	δCCN (18)	-	-	102
6	τCNNC (12) + τCCNN (10) + τSCCC (14)	-	-	120
7	τCNNC (2) + τCCCN (15) + τSCCC (11)	-	-	152
8	δNNC (13)	-	-	227
9	τCCCN (14) + τNNCC (17) + τSCCC (10)	-	-	261
10	τCCNN (34) + τSCCC (33)	-	-	365
11	δCCN (14) + δCCN (10)	-	-	454
12	τHNNC (81)	-	-	530
13	νSC (12) + δSCC (53)	-	-	634
14	τHCCS (20)	617	623	639
15	τHCSC (52) + τHCSC (39)	-	-	684
16	δCCN (15)	-	-	750
17	τHCSC (40) + τHCSC (30)	772	-	780
18	νSC (27)	848	-	857
19	νSC (12)	867	-	872
20	νSC (14)			877
21	τHCCS (62) + τHCSC (18)			908
22	τHCNN (88)	922	-	955
23	νNN (10)	-	-	1072
24	δHCS (36) + δHCS (36)	-	-	1109
25	νNN (30)	1092	1095	1147
26	δHCS (14)	1126	1129	1178
27	νNN (14) + δHCS (43)	1165	1158	1202
28	δHCS (30)	1236	1238	1274
29	δHCN (57)	-	-	1371
30	δHNN (27)	-	1524	1559
31	δHNN (16)	-	1524	1560
32	δHNN (24)	-	-	1587
33	νNC (71) + δHCN (11)	1602	1606	1677
Linear correlation coefficients (R^2)		0.999133	0.999211	

ν : stretching. δ : bending. τ : torsion. γ : out of plane bending

Table S17. Main Electronic transitions of the calculated UV spectra of **LASSBio-294 (1)** and **LASSBio-897 (2)**.

Compound	Transition	Wavelength (nm)	Oscillator Strength > 0.1
LASSBio-294 (1)	(HOMO → LUMO) 71 → 72	340.54	0.8242
	70 → 72	310.28	0.1777
	68 → 72	259.41	0.1198
	70 → 73		
	71 → 73		
	71 → 74		
	67 → 73	208.02	0.4667
	69 → 73		
	70 → 74		
	71 → 74		
	71 → 76		
LASSBio-897 (2)	(HOMO → LUMO) 71 → 72	318.00	0.8146
	70 → 72	289.11	0.2806
	71 → 73		
	67 → 72	252.29	0.1031
	69 → 72		
	70 → 72		
	71 → 73		
	71 → 74		
	67 → 72	242.49	0.1706
	69 → 72		
	70 → 73		
	71 → 73		

Chemistry. LASSBio-294 (1) and LASSBio-897 (2) were synthesized according to the proceedings described in Kümmerle, *et al* (2009).¹⁷

(2-Thienylidene)3,4-methylenedioxybenzoylhydrazine (LASSBio-294). mp 205 °C. ¹H NMR data are in agreement with those previously published.¹⁸ ¹³C NMR (100 MHz): δ 102.6, 107.9, 108.4, 123.1, 127.4, 128.2, 129.2, 131.2, 139.5, 142.9, 147.7, 150.5, 162.4. LRMS calculated for C₁₃H₁₀N₂O₃S: [M]⁺ = 274.04. Found: [M + H]⁺ = 275.13. 99.1% purity in HPLC, t_r = 3.77 min (λ = 254 nm).

(3-Thienylidene)3,4-methylenedioxybenzoylhydrazine (LASSBio-897). mp 195 °C. ¹H NMR (400 MHz): δ 11.58 (s, 1H), δ 8.47 (s, 1H), δ 7.92 (d, 1H, *J* = 1.70 Hz), δ 7.64 (dd, 1H, *J* = 5.00, 1.70 Hz), δ 7.52 (dd, 1H, *J* = 8.00, 1.70 Hz), δ 7.49 (d, 1H, *J* = 5.00 Hz), δ 7.44 (d, 1H, *J* = 1.70 Hz), δ 7.06 (d, 1H, *J* = 8.00 Hz), δ 6.13 (s, 2H). ¹³C NMR (100 MHz): δ 102.6, 107.9, 108.4, 123.1, 125.0, 127.9, 128.0, 128.5, 137.9, 143.5, 147.7, 150.5, 162.5. LRMS calculated for C₁₃H₁₀N₂O₃S: [M]⁺ = 274.04. Found: [M + H]⁺ = 275.13. 98.9 % purity in HPLC, t_r = 3.60 min (λ = 254 nm).

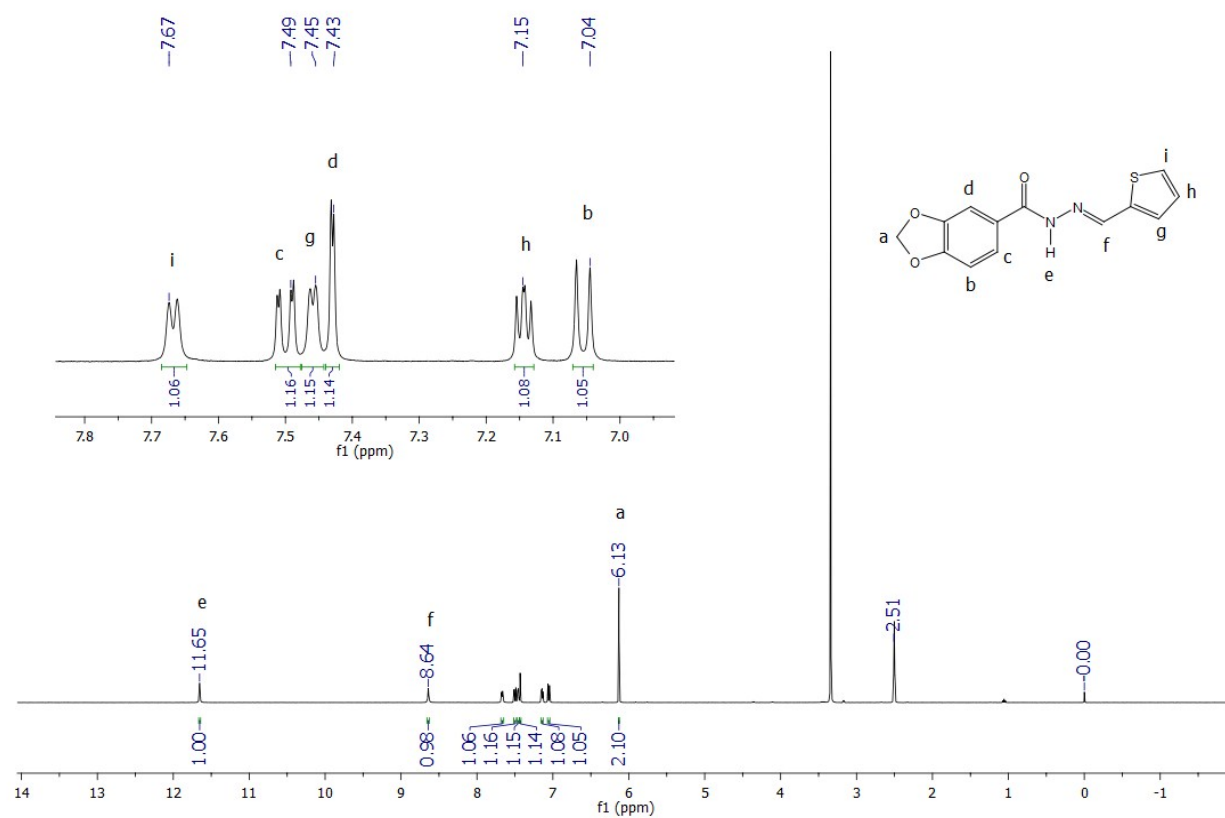


Figure S14. ^1H -NMR spectra of compound **LASSBio-294 (1)**, 400 MHz, $\text{DMSO}-d_6$.

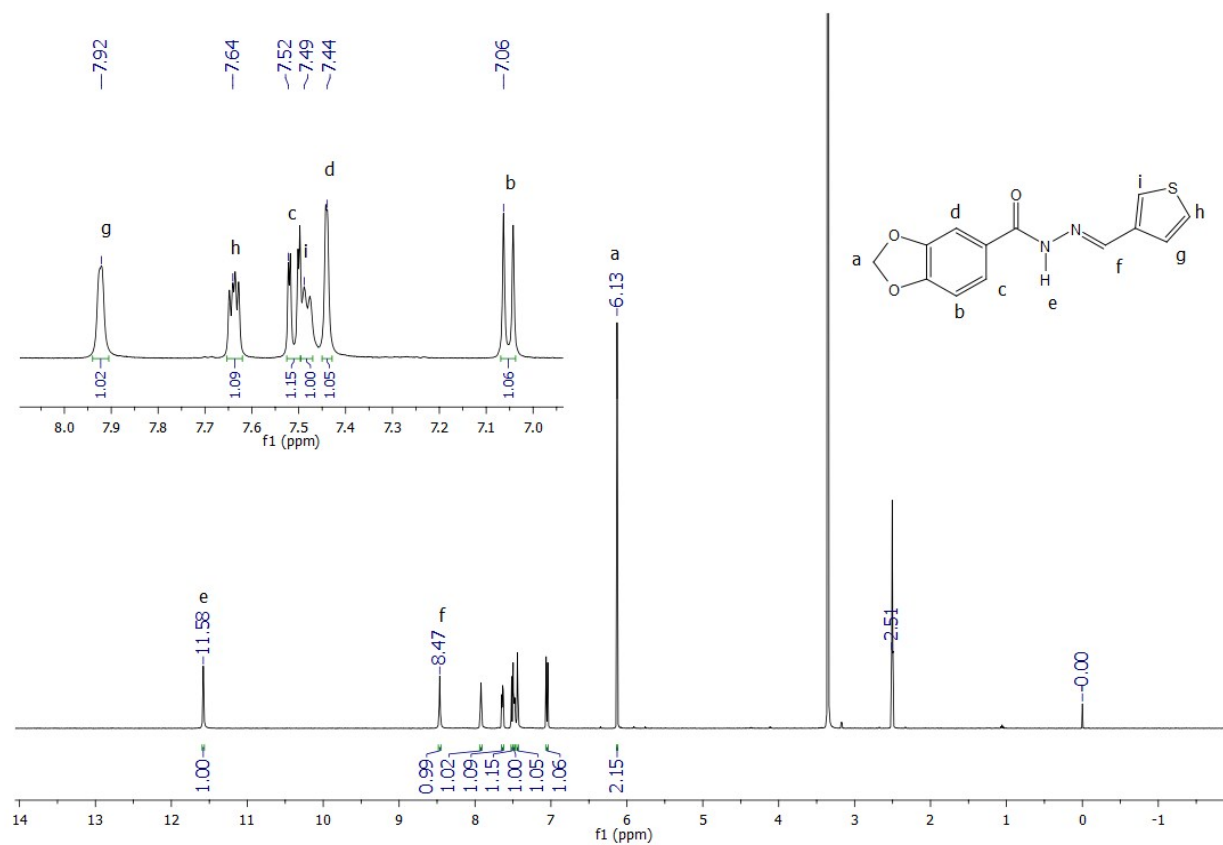


Figure S15. ^1H -NMR spectra of compound **LASSBio-897 (2)**, 400 MHz, $\text{DMSO}-d_6$.

5. Spectroscopy acquisition details.

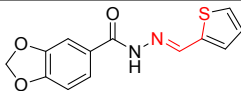
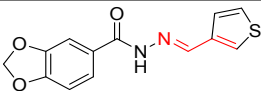
5.1. NMR spectroscopy. All NMR spectra were acquired at 25°C, using a 5-mm inverse detection z-gradient probe. NMR samples (30 mg) were dissolved in DMSO- d_6 with 0.05% tetramethylsilane as an internal reference for ^1H and ^{13}C chemical shifts (0 ppm). For the ^{15}N chemical shift reference (0 ppm), nitromethane was added as an internal reference with the same molarity as the samples. 2D NOESY (Nuclear Overhauser Spectroscopy) spectra were acquired with 1 second of mixing time, 16 scans and 2K points in F2 and 200 points in F1 on a 500 VNMRS (Agilent) at 499.78 MHz for ^1H . The heteronuclear single quantum correlation (HSQC) and heteronuclear multiple-bond correlation (HMBC) spectra were recorded using a standard Varian protocol on a Varian MR-400 spectrometer operating at 399.74 MHz for ^1H , with 32 or 64 scans, 1K points in F2 and 200 points in F1. The delay for the evolution of long range couplings was 62.5 ms (8 Hz) for (^1H - ^{13}C) HMBC and 100 ms (5 Hz) for (^1H - ^{15}N) HMBC. All NMR spectra were processed with the MestreNova 9.0.1 program.

5.2. Vibrational characterization. The FT-IR (ATR) spectra of the samples were recorded at room temperature using a Varian 660 spectrometer from 4000 – 600 cm^{-1} with a resolution of 4 cm^{-1} . The FT-Raman spectra of the samples were recorded by a Bruker MultiRam spectrometer at room temperature with a germanium detector, maintained at liquid nitrogen temperature, using the 1064 nm Nd-YAG laser line with a resolution of 2 cm^{-1} in the region of 4000 – 200 cm^{-1} .

5.3. UV spectroscopy. The ultraviolet spectra were recorded at room temperature using a Femto 800 XI spectrophotometer with 0.5 nm resolution from 245 – 450 nm, using DMSO as the solvent.

6. Additional theoretical data.

Table S18. The Cartesian coordinates of **LASSBio-294 (1)** and **LASSBio-897 (2)**.

							
atom	X	Y	Z	atom	X	Y	Z
C	2.735494	0.790454	-0.205987	N	0.466918	-0.149889	-0.045225
H	2.443565	1.809382	-0.495541	C	-0.565792	0.765045	-0.223495
C	4.153883	0.522698	-0.182397	N	1.760447	0.242600	-0.119008
C	6.421387	-0.469236	0.019810	C	-1.938660	0.161464	-0.181546
H	7.252042	-1.140020	0.184856	O	-0.377236	1.950858	-0.384995
C	6.460089	0.840913	-0.367889	C	2.660139	-0.617484	0.181698
H	7.378624	1.380530	-0.562866	C	-2.208069	-1.167461	-0.522957
C	5.163761	1.408731	-0.483197	C	-2.991148	1.034256	0.167675
H	4.975860	2.435208	-0.776955	C	4.073097	-0.281069	0.113391
C	-0.442080	-0.697628	0.220544	C	-3.513510	-1.681704	-0.507087
C	-1.830637	-0.130181	0.188511	C	-4.260818	0.512975	0.188600
C	-2.135112	1.185454	0.551202	C	4.585941	1.003390	-0.273390
H	-1.354357	1.849797	0.904434	C	5.078626	-1.168418	0.413845
C	-3.452858	1.667406	0.534310	C	-4.520733	-0.816803	-0.137973
H	-3.692510	2.681847	0.829010	O	-5.439120	1.151280	0.480563
C	-4.435477	0.784619	0.142006	C	5.943305	1.054342	-0.254660
C	-6.354276	-0.234131	-0.411370	S	6.644326	-0.461040	0.233687
H	-7.078844	-0.585643	0.327635	O	-5.863183	-1.059082	-0.061696
H	-6.824494	-0.077926	-1.386348	C	-6.449816	0.139626	0.468645
C	-4.140725	-0.532434	-0.204646	H	2.401181	-1.637159	0.498668
C	-2.858698	-1.022603	-0.183230	H	-1.408606	-1.819091	-0.857510
H	-2.623870	-2.049730	-0.430163	H	-2.783811	2.071953	0.394169
N	0.563057	0.249918	0.048214	H	-3.725813	-2.706086	-0.788015
H	0.313052	1.177049	-0.281302	H	3.944881	1.831674	-0.543918
N	1.868360	-0.104918	0.091542	H	4.983167	-2.198234	0.726970
O	-0.219103	-1.879016	0.366004	H	6.585266	1.888850	-0.495087
O	-5.297019	-1.189871	-0.536576	H	-7.271486	0.453593	-0.176540
O	-5.779836	1.002587	0.040397	H	-6.793769	-0.049066	1.491592
S	4.803136	-1.040592	0.252772	H	0.249162	-1.082169	0.292866

CORRESPONDING AUTHOR

*To whom correspondence should be addressed. Email: cmfraga@ccsdecania.ufrj.br

AUTHOR CONTRIBUTIONS

The manuscript was written through contributions of all authors. All authors have given approval to the final version of the manuscript.

FUNDING SOURCES

This work was funded by CAPES (Coordenação de Aperfeiçoamento de Pessoal de Nível Superior), CNPq (Conselho Nacional de Desenvolvimento Científico e Tecnológico), INCT-Inofar (Instituto Nacional de Ciência e Tecnologia de Fármacos e Medicamentos) and FAPERJ (Fundação de Amparo à Pesquisa do Estado do Rio de Janeiro).

ACKNOWLEDGMENT

The authors would like to thank the multi-user analysis laboratories LAMAR (Laboratório Multiusuário de Análises por RMN – Instituto de Pesquisas de Produtos Naturais, UFRJ) and LAME (Laboratório Multiusuário de Espectroscopia – UFF) for the realization of the NMR and the IR and Raman experiments, respectively.

REFERENCES

- 1 B. R. Beno, K.-S. Yeung, M. D. Bartberger, L. D. Pennington and N. A. Meanwell, *J. Med. Chem.*, 2015, **58**, 4383–4438.
- 2 H. Gökce and S. Bahçeli, *J. Mol. Struct.*, 2011, **1005**, 100–106.
- 3 R. Ghosh and S. H. Simonsen, *Acta Crystallogr. Sect. C Cryst. Struct. Commun.*, 1993, **49**, 1031–1032.
- 4 J. J. P. Stewart, *J. Mol. Model.*, 2007, **13**, 1173–1213.
- 5 A. D. Becke, *Phys. Rev. A*, 1988, **38**, 3098–3100.
- 6 C. Lee, W. Yang and R. G. Parr, *Phys. Rev. B*, 1988, **37**, 785–789.
- 7 E. J. Barreiro, A. E. Kümmerle and C. A. M. Fraga, *Chem. Rev.*, 2011, **111**, 5215–5246.
- 8 D. C. Young, *Computational Chemistry*, John Wiley & Sons, Inc., New York, USA, 2001, vol. 31.
- 9 R.-J. Chein and E. J. Corey, *Org. Lett.*, 2010, **12**, 132–135.
- 10 and D. J. F. M. J. Frisch, G. W. Trucks, H. B. Schlegel, G. E. Scuseria, M. A. Robb, J. R. Cheeseman, G. Scalmani, V. Barone, G. A. Petersson, H. Nakatsuji, X. Li, M. Caricato, A. Marenich, J. Bloino, B. G. Janesko, R. Gomperts, B. Mennucci, H. P. Hratchian, J. V. Ort, 2009.
- 11 F. WEINHOLD and C. R. LANDIS, *Chem. Educ. Res. Pr.*, 2001, **2**, 91–104.
- 12 J. S. Murray, P. Lane and P. Politzer, *Int. J. Quantum Chem.*, 2008, **108**, 2770–2781.
- 13 R. Rittner, L. C. Ducati, C. F. Tormena, B. C. Fiorin and C. B. Braga, *Spectrochim. Acta Part A Mol. Biomol. Spectrosc.*, 2011, **79**, 1071–1076.
- 14 F. Zhou, R. Liu, J. Tang, P. Li, Y. Cui and H. Zhang, *J. Mol. Model.*, 2016, **22**, 29.
- 15 M. H. Jamróz, *Spectrochim. Acta Part A Mol. Biomol. Spectrosc.*, 2013, **114**, 220–230.
- 16 I. Kondolff, H. Doucet and M. Santelli, *J. Mol. Catal. A Chem.*, 2007, **269**, 110–118.
- 17 A. E. Kümmerle, J. M. Raimundo, C. M. Leal, G. S. da Silva, T. L. Balliano, M. A. Pereira, C. A. de Simone, R. T. Sudo, G. Zapata-Sudo and C. A. M. Fraga, *Eur. J. Med. Chem.*, 2009, **44**, 4004–4009.
- 18 A. G. Silva, G. Zapata-Sudo, A. E. Kummerle, C. A. M. Fraga, E. J. Barreiro and R. T. Sudo, *Bioorg. Med. Chem.*, 2005, **13**, 3431–3437.
- 19 J. A. P. Sato, F. N. Costa, M. D. da Rocha, E. J. Barreiro, C. A. M. Fraga, F. Punzo and F. F. Ferreira, *CrystEngComm*, 2015, **17**, 165–173.